ChemPlusChem

Research Article
doi.org/10.1002/cplu.202400410

Chemistry Europe
European Chemical Societies Publishing

www.chempluschem.org

Stereocontrol of Metal-Centred Chirality in Rhodium(III) and Ruthenium(II) Complexes with $N_2N'P$ Ligand

Irati Barriendos,[a] Íber Almárcegui,[a] María Carmona,[a] Alvaro G. Tejero,[a] Alejandro Soriano-Jarabo,[a] Carlota Blas,[a] Zulima Aguado,[a, b] Daniel Carmona,[a] Fernando J. Lahoz,[a] Pilar García-Orduña,[a] Fernando Viguri,*[a] and Ricardo Rodríguez*[a]

Rh(III) and Ru(II) complexes, $[RhCl_2(\kappa^4\text{-}N_2N'P\text{-}\mathbf{L})][SbF_6]$ (**1**) and $[RuCl_2(\kappa^4\text{-}N_2N'P\text{-}\mathbf{L})]$ (**2**), were synthesised using the tetradentate ligand **L** (**L** = *N*,*N*-bis[(pyridin-2-yl)methyl]-[2-(diphenylphosphino)phenyl]methanamine). In each case only one diastereomer is detected, featuring *cis*-disposed pyridine groups. The chloride ligand *trans* to pyridine can be selectively abstracted by $AgSbF_6$, with the ruthenium complex (**2**) reacting more readily at room temperature compared to the rhodium complex (**1**) which requires elevated temperatures. Rhodium complexes avoid the second chloride abstraction, whereas ruthenium complexes can form the chiral bisacetonitrile complex $[Ru(\kappa^4\text{-}N_2N'P\text{-}\mathbf{L})(NCMe)_2][SbF_6]_2$ (**5**) upon corresponding treatment with $AgSbF_6$. The complex $[RhCl_2(\kappa^4\text{-}N_2N'P\text{-}\mathbf{L})][SbF_6]$ (**1**) has also been used to synthesise polymetallic species, such as the tetrametallic complex $[\{RhCl_2(\kappa^4\text{-}N_2N'P\text{-}\mathbf{L})\}_2(\mu\text{-}Ag)_2][SbF_6]_4$ (**6**) which was formed with complete diastereoselectivity and chiral molecular self-recognition. In addition, a stable bimetallic mixed-valence complex $[\{Rh(\kappa^4\text{-}N_2N'P\text{-}\mathbf{L})\}\{Rh(COD)\}(\mu\text{-}Cl)_2][SbF_6]_2$ (**7**) (COD = cyclooctadiene) was synthesised. These results highlight the significant differences in chloride lability between Rh^{3+} and Ru^{2+} complexes and demonstrate the potential for complexes to act as catalyst precursors and ligands in further chemistry applications.

Introduction

In asymmetric catalysis, the primary source of catalyst chirality has traditionally been chiral organic molecules with stereogenic carbon atoms or those exhibiting atropoisomerism.[1] Consequently, the predominant design of an asymmetric metal catalyst involves the use of an enantiopure chiral ligand. Numerous enantiopure ligands with diverse stereoelectronic properties have been developed and continue to be refined for coordination to metal centres, achieving very high enantioselectivities in a wide range of catalytic processes. Recently, there has been considerable interest in the application of asymmetric catalysis to chiral metal complexes with non-chiral ligands.[2] Among the few studies conducted on the synthesis of chiral-at-metal catalysts, most examples described are octahedral complexes, although some tetrahedral complexes have also been explored.[3]

Chiral octahedral complexes have been known since 1911 when Werner reported $[Co(en)_3]^{3+}$ (en = ethylenediamine) (**I**, Scheme 1).[4] Recently, Gladysz and co-workers prepared Werner-type Co(III) complexes with three achiral bidentate ligands and demonstrated their efficacy as enantioselective catalysts.[5]

Meggers and co-workers have prepared cyclometalated Rh(III) and Ir(III)[6] complexes of octahedral geometry (**II**, Scheme 1) in which two monoanionic bidentate C^N ligands (5-tert-butyl-2-phenylbenzoxazole) occupy four of the six coordination sites of the metal atom. Due to a strong preference for the configuration in which both nitrogen atoms are *trans* to each other, the complexes form with perfect diastereoselectivity, yielding five-membered metallacycles that confer significant stability to the metal complex. Once resolved, these complexes have been used as enantioselective catalysts. In the search for new metal-centred chiral catalysts, Meggers' group has explored other octahedral complexes based on Ru(II),[7] Fe(II)[8] (**III**) and Os(II)[9] (**VI**) with two *N*-heterocyclic carbene-pyridine ligands coordinated in a bidentate manner. These ligands confer great configurational stability to the complex, yielding only one diastereomer with the pyridine groups in the *trans* position. In addition, ruthenium catalysts **VI** lacking C_2 symmetry have been diastereoselectively synthesised containing two cyclometalated 7-methyl-1,7-phenanthroline heterocycles, which can be described as two pyridine-carbene chelate ligands with the pyridine and carbene in *trans* positions.

In 2018, we reported an enantioselective catalytic metal system in which the octahedral complex exhibits metal-centred chirality using achiral ligands.[10] To address the stereochemical control of the six metal coordination positions, we used a

[a] I. Barriendos, Í. Almárcegui, M. Carmona, A. G. Tejero, A. Soriano-Jarabo, C. Blas, Z. Aguado, D. Carmona, F. J. Lahoz, P. García-Orduña, F. Viguri, R. Rodríguez
Instituto de Síntesis Química y Catálisis Homogénea (ISQCH), CSIC-Universidad de Zaragoza, Departamento de Química Inorgánica, Pedro Cerbuna 12, 50009 Zaragoza, Spain
E-mail: fviguri@unizar.es
riromar@unizar.es

[b] Z. Aguado
Universidad San Jorge, Department of Pharmacy, Faculty of Health Sciences, 50830 Villanueva de Gállego (Zaragoza), Spain

Supporting information for this article is available on the WWW under https://doi.org/10.1002/cplu.202400410

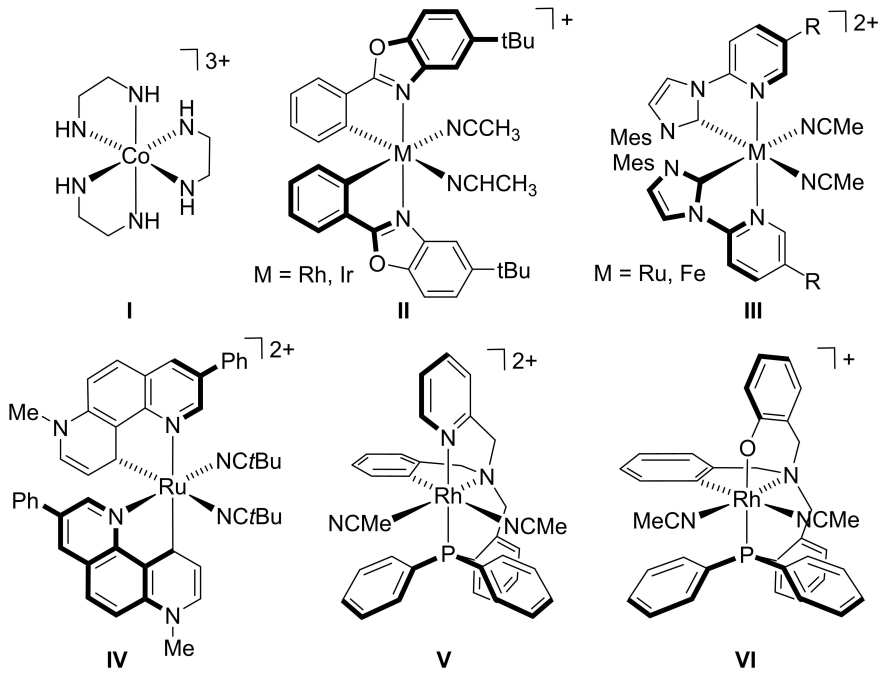

Scheme 1. Chiral-at-metal catalysts.

tripodal achiral tetradentate ligand to diastereoselectively prepare chiral octahedral complexes of Rh(III)[11] (**V**, Scheme 1) and Ru(II)[12]. The coordination atoms of the tetradentate ligand include two nitrogen atoms (one from the sp^3 amine and the other from pyridine), one phosphorus atom from the arylphosphine group and one carbon atom from the cyclometalated aryl group. The synthetic route is highly diastereoselective: only a single isomer is detected and isolated, in which the phosphorus and pyridine nitrogen are mutually in *trans*. Recently, we have successfully synthesised and resolved the chiral-at-rhodium complex **VI** based on the tetradentate ligand,[13] which exhibits a dynamic configuration at the rhodium centre at room temperature without loss of chiral information. This dynamic configuration is mediated by a non-dissociative mechanism involving a concerted transition state with trigonal bipyramidal geometry.

In this work we present a fully diastereoselective synthetic route to obtain chiral rhodium and ruthenium dichlorido complexes of formula $[RhCl_2(\kappa^4\text{-}N_2N'P\text{-}\mathbf{L})][SbF_6]$ (**1**) and $[RuCl_2(\kappa^4\text{-}N_2N'P\text{-}\mathbf{L})]$ (**2**), where $N_2N'P$-**L** represents the coordinated tripodal tetradentate ligand shown in Scheme 2. A detailed study of the dichloride abstraction reaction using silver hexafluoroantimonate reveals significant differences in chloride lability reactivity between the two metals. This enables two types of potential applications, with the ruthenium complex acting as a catalyst and the rhodium as a ligand in polymetallic complexes.

Results and Discussion

Synthesis and Characterization of Dichloride Complexes $[RhCl_2(\kappa^4\text{-}N_2N'P\text{-}\mathbf{L})][SbF_6]$ (1) and $[RuCl_2(\kappa^4\text{-}N_2N'P\text{-}\mathbf{L})]$ (2)

The tetradentate ligand **L** (Scheme 2) was synthesized as previously reported. One-pot reductive amination of 2-diphenylphosphino benzaldehyde with di-(2-picolyl)amine in the

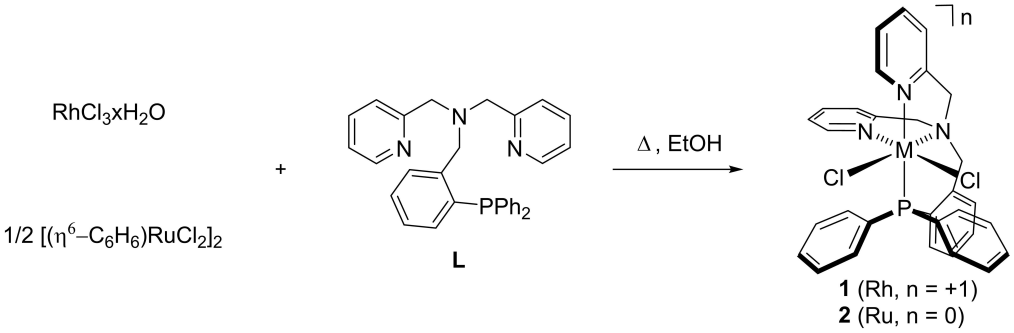

Scheme 2. Synthesis dichlorido complexes **1** and **2**.

presence of an excess of $NaBH(OAc)_3$ afforded the ligand in high overall yield.[14]

Dichloride complex **1** was prepared by treating $RhCl_3 \cdot xH_2O$ with a molar equivalent of the ligand **L** in refluxing ethanol overnight (Scheme 2). For ruthenium complex **2**, a suspension of $[(\eta^6\text{-}C_6H_6)RuCl_2]_2$ and the ligand **L** was treated under argon in ethanol, refluxing overnight.[12] The long reaction times required may be due to the low solubility of the reagents and products under the reaction conditions.

Analytical and spectroscopic data indicate that the isolated solids consist of only one diastereomer derived from the tetradentate coordination of ligand **L** ($\kappa^4\text{-}N_2N'P$) to Rh(III) and Ru(II) through the three nitrogen and phosphorus atoms, with two chlorides in the *cis* position. From a stereochemical point of view, with the tetradentate coordination mode of ligand **L**, two diastereomers are possible. In the octahedral fragments $\{MCl_2(\kappa^4\text{-}N_2N'P\text{-}\mathbf{L})\}$ (M=Rh, Ru), *fac* coordination of the three nitrogen atoms results in a chiral complex with a stereogenic metal centre. However, if the coordination mode is *mer*, no chiral complex will be formed. The two possible diastereomers of complexes **1** and **2** are depicted in Scheme 3.[15]

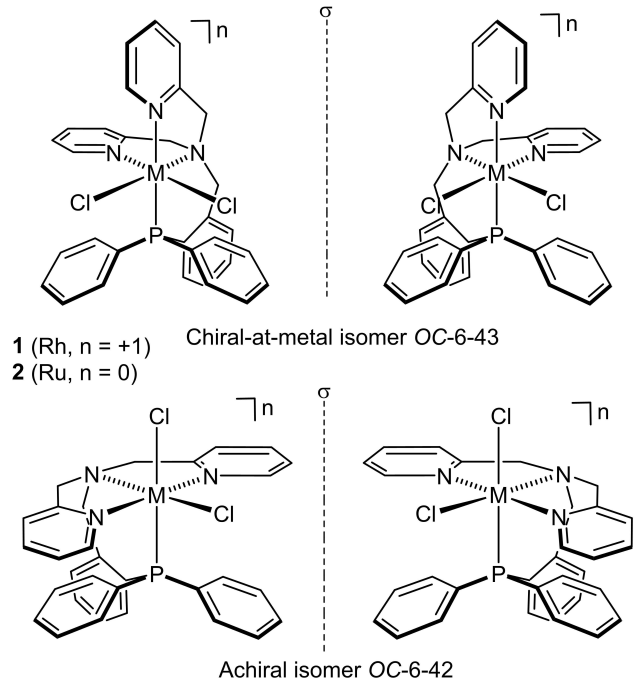

Scheme 3. Dichlorido isomers.

The new complexes were characterised by analytical and spectroscopic methods (see Experimental Section). The assignment of the NMR signals was verified using two-dimensional homonuclear and heteronuclear correlation techniques. The $^{31}P\{^1H\}$ NMR spectrum consists of a doublet at 30.66 ppm with a coupling constant ($J_{103Rh\text{-}31P}$) of 107.6 Hz for complex **1**. In the ^1H NMR spectrum for complex **1** shown in Figure 1, the six protons of the three methylene groups, each with a distinct chemical shift, are observed between 3.5 and 5.7 ppm (see Experimental Section). The absence of equivalent CH_2 protons confirms the chiral nature of the complex **1**, which lacks a plane of symmetry. Similarly, each signal assigned to the two protons at position 6 of the pyridine groups (6-CH(Py)) displays a distinct multiplicity and chemical shift: one appears at 9.11 ppm as a pseudo-triplet ($J_{31P\text{-}1H}$ = 2.4 Hz) and the other at 8.51 ppm as a doublet ($J_{1H\text{-}1H}$ = 5.3 Hz). The difference in the coupling constants on the 6-CH(Py) protons can be attributed to the *cis* position of the two pyridine groups, resulting in higher coupling when the phosphorus atom is in the *trans* position to a pyridine (Py_{transP}). These findings can be applied to all the complexes studied, distinguishing the chiral-at-metal isomer from the achiral isomer. The value of the $J_{31P\text{-}1H}$ coupling constant, along with COSY, HSQC and HMBC experiments, allows the assignment of the six protons, labelled as $CH_2(P)$, $CH_2(Py_{transP})$ and $CH_2(Py_{cisP})$. The NOE relationship pattern for the six methylene protons (Scheme 4) is only compatible with the chiral-at-metal *OC*-6-43 isomer (Scheme 3), where the phosphorus and the pyridine nitrogen atoms are mutually in *trans*.

For the ruthenium complex **2**, the $^{31}P\{^1H\}$ NMR spectrum shows only one singlet centred at 58.76 ppm. The proton NMR of **2** shows six signals for each methylene proton and two signals for the 6-CH(Py_{transP}) (9.62 ppm, t, J = 2.0 Hz) and 6-CH(Py_{cisP}) (8.53 ppm, d, J = 4.7 Hz) protons, indicating that the obtained isomer is the chiral one. The proposed isomer of **2** is different from the one reported by Jia *et al.* for the parent

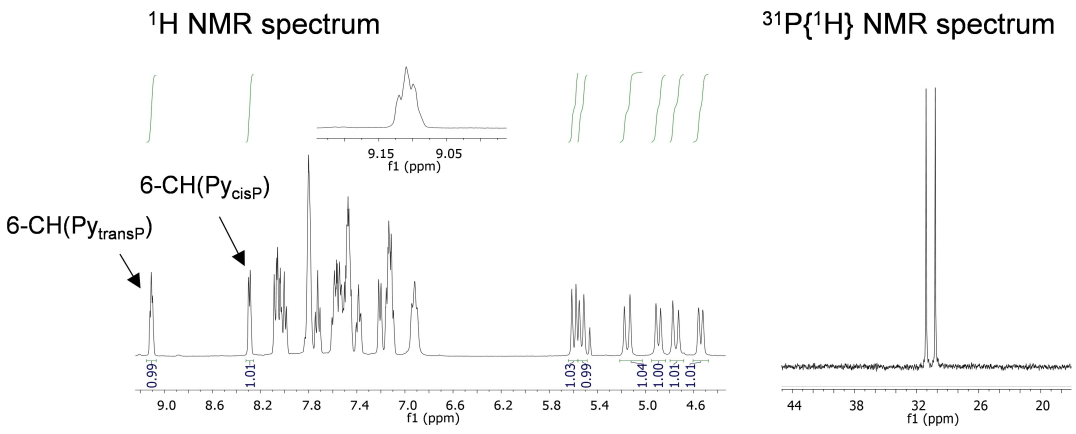

Figure 1. ^1H and $^{31}P\{^1H\}$ NMR spectra of complex **1** in CD_2Cl_2.

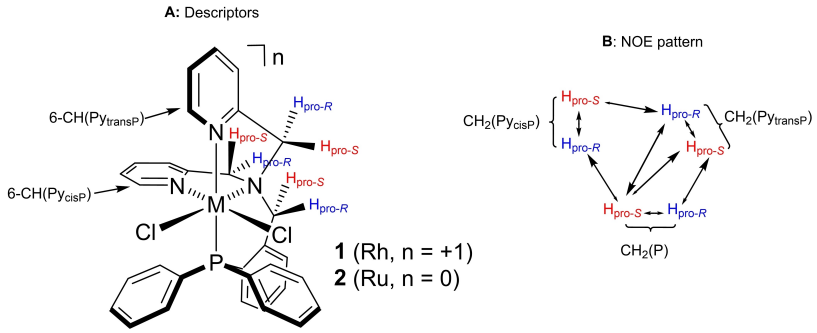

Scheme 4. Assignment of the descriptors and NOE relationship pattern on *OC*-6-43-*C* isomer.

complex with the same ligand [Ru(OAc)(κ^4-$N_2N'P$-**L**)][BPh_4],[14,16] where the non-chiral isomer is formed. However, when this complex reacts with phenylacetylene and H_2O at 80 °C, the chiral-at-metal isomer [Ru(CH_2Ph)(CO)(κ^4-$N_2N'P$-**L**)][BPh_4] is obtained. We, therefore, propose that since the reaction of **2** is carried out in refluxing ethanol, the isomer obtained is likely to be the thermodynamic one, corresponding to the chiral *OC*-6-43 isomer.

Single crystals of complexes **1** and **2**, were prepared from dichloromethane solutions and analysed by X-ray diffraction.[17] Figure 2 shows the molecular structure of the complexes (only one of the two enantiomers is shown) and Table 1 lists the relevant structural parameters of the metal coordination spheres. Both molecular structures exhibit an octahedral coordination geometry around the central metal atom. Two chloride ligands occupy *cis* coordination sites, while the four donor atoms of the tetradentate ligand **L** complete the coordination sphere. According to the NMR data, the phosphorus atom is *trans* to the pyridine nitrogen N(1), while the chlorine atoms Cl(1) and Cl(2) are *trans* to the pyridine nitrogen N(2) and the amine nitrogen N(3), respectively. In complex **1**, the bond lengths Rh–Cl(1) (2.3361(7) Å) and Rh–Cl(2) (2.3359(7) Å) show no significant differences. In complex **2**, however, the difference in bond length between Ru–Cl(1) (2.4341(3) Å) and Ru–Cl(2) (2.4580(3) Å) is attributed to the stronger *trans* influence of the pyridine nitrogen N(1) compared to the sp^3 nitrogen N(3).[18] In addition, the *trans* influence of phosphine compared to the pyridine nitrogen is observed in the bond lengths Rh–N(1) (2.073(2) Å) and Rh–N(2) (2.102(2) Å) in complex **1** and Ru–N(1) (2.1031(9) Å) and Ru–N(2) (2.1341(9) Å) in complex **2**, respectively.

Synthesis and Characterisation of Complexes [MCl(κ^4-$N_2N'P$-L)(NCMe)][SbF_6]$_n$, M=Rh (3), n = +2; Ru (4), n = +1

Silver salt metathesis is a widely used method to obtain suitable catalyst precursors. This process replaces the chloride ligands in these complexes with more labile ligands, such as solvent molecules, generating transition-metal fragments with vacant sites. However, despite its widespread use, the method has shortcomings, including incomplete chloride abstraction lead-

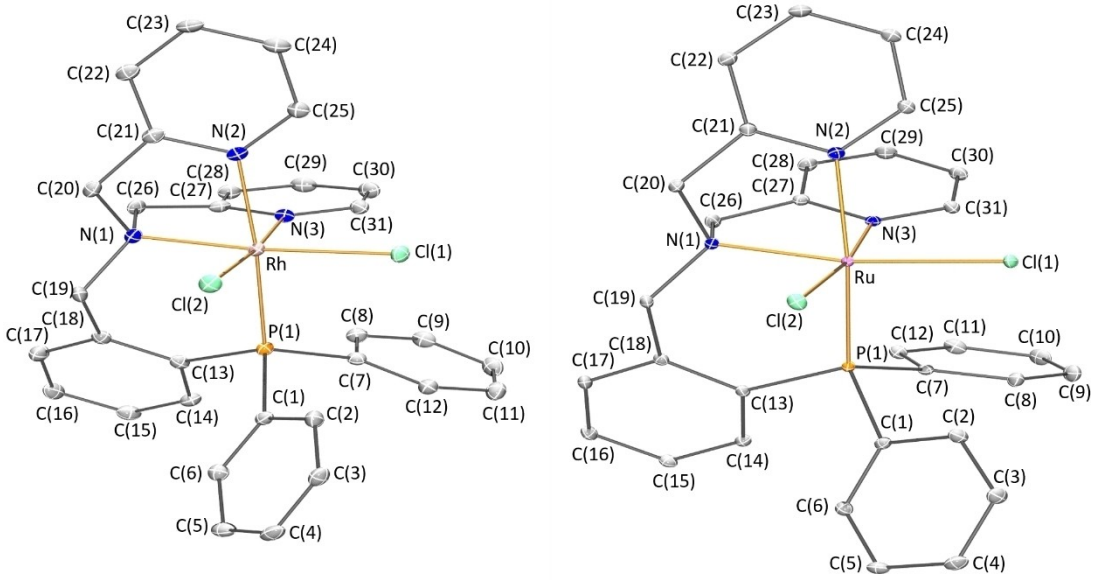

Figure 2. Molecular structure of the complexes **1**·CH_2Cl_2 (left) and **2**·CH_2Cl_2 (right). For clarity, hydrogen atoms and solvate molecules have been omitted.

Table 1. Selected bond lengths (Å) and angles (°) for complexes **1**·CH_2Cl_2 and **2**·CH_2Cl_2.

	1	2		1	2
M–Cl(1)	2.3361(7)	2.4341(3)	Cl(2)–M–P	94.94(3)	93.259(12)
M–Cl(2)	2.3359(7)	2.4580(3)	Cl(2)–M–N(1)	92.11(6)	90.95(3)
M–P	2.2915(7)	2.2408(3)	Cl(2)–M–N(2)	87.05(6)	94.04(3)
M–N(1)	2.073(2)	2.1031(9)	Cl(2)–M–N(3)	174.59(7)	172.14(3)
M–N(2)	2.102(2)	2.1341(9)	P–M–N(1)	94.09(7)	93.73(3)
M–N(3)	2.040(2)	2.0453(12)	P–M–N(2)	174.25(7)	170.23(3)
Cl(1)–M–Cl(2)	89.41(3)	90.957(12)	P–M–N(3)	88.78(7)	92.20(3)
Cl(1)–M–P	91.04(3)	95.721(12)	N(1)–M–N(2)	80.43(9)	79.68(4)
Cl(1)–M–N(1)	174.50(6)	170.24(3)	N(1)–M–N(3)	83.68(9)	83.05(4)
Cl(1)–M–N(2)	94.38(7)	90.64(3)	N(2)–M–N(3)	88.89(9)	79.92(3)
Cl(1)–M–N(3)	94.46(7)	94.13(3)			

ing to binuclear bridged chloride complexes or the formation of silver-containing heteronuclear complexes.[19]

The synthesis of complexes [MCl(κ^4-$N_2N'P$-**L**)(NCMe)][SbF_6]$_n$ M=Rh (**3**), n = +2; Ru (**4**), n = +1 were conducted in acetonitrile in the presence of $AgSbF_6$ (molar ratio 1/1). During the reaction time, a suspension of AgCl was formed in the medium, and from the filtered solutions, the new cationic complexes were isolated: [RhCl(κ^4-$N_2N'P$-**L**)(NCMe)][SbF_6]$_2$ (**3**) in 80% yield and [RuCl(κ^4-$N_2N'P$-**L**)(NCMe)][SbF_6] (**4**) in 90% yield, as depicted in Scheme 5. Notably, the chloride ligand abstraction reaction of cationic rhodium **3** requires 4 days of heating at 60 °C, whereas the reaction for neutral ruthenium complex **4** takes place in 4 h at room temperature. This significant difference in behaviour highlights the distinct nature of the metal centres concerning the formal charge, Lewis acidity, and the relative ligand dissociation ability of complexes **3** and **4**.

The complexes were fully characterised by analytical and spectroscopic methods (see Experimental Section). The NMR spectra of complexes **3** and **4** consist of a single set of sharp resonance signals, indicating perfect selectivity of the reaction. The ^{31}P NMR spectra for **3** and **4** in CD_2Cl_2, show only one doublet at 28.80 ppm (d, J = 98.2 Hz) and singlet at 55.79 ppm, respectively. The ^{1}H NMR spectra present six signals for methylene protons of ligand **L** coordinated to the metal centre, and different chemical shifts for the 6-CH(Py): *trans* (Rh, 8.98 ppm, t, J = 4.3 Hz); (Ru, 9.31 ppm, m) and *cis* (Rh, 8.25 ppm, d, J = 6.1 Hz); (Ru, 8.68 ppm, d, J = 6.1 Hz) to the phosphorus atom. These indicate the complete selectivity of the reaction to one isomer of **3** and **4**.

The ^{1}H-^{31}P HMBC experiment of complex **3** correlates the proton signal at 1.93 ppm, assigned to coordinated acetonitrile, with the phosphorus signal, confirming acetonitrile coordination to the rhodium atom. Similar observations were made for ruthenium complex **4**, and the phosphorous signal correlates with the methyl group of NCMe at 1.85 ppm. The mass spectrometry agrees with the presence of the fragment {MCl(κ^4-$N_2N'P$-**L**)(NCMe)} with only one coordinated chloride atom. For both complexes, **3** and **4**, the NOESY spectra show interactions between the acetonitrile methyl protons and CH_2(P) and CH_2(Py_{transP}) groups, confirming that the formed and isolated monochlorido complex [MCl(κ^4-$N_2N'P$-**L**)(NCMe)][SbF_6]$_n$ (M=Rh (**3**), n = +2; Ru (**4**), n = +1) is the isomer in which the NCMe ligand is in *trans* disposition to the pyridine ring (Scheme 5).

Single crystals of **4**, suitable for X-ray analysis, were obtained from dichloromethane solutions of the compound. The structure of the complex cation is depicted in Figure 3, and relevant characteristics of the metal coordination sphere are summarised in Table 2. Complex **4** features a stereogenic ruthenium in an octahedral geometry, coordinated by the ligand **L** (κ^4-$N_2N'P$), a chloride ligand, and an acetonitrile group.

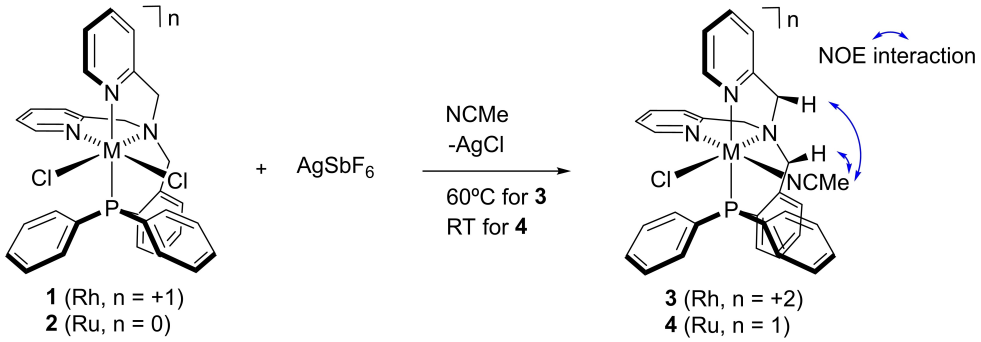

Scheme 5. Synthesis of monoacetonitrile complexes **3** and **4** and NOE interactions.

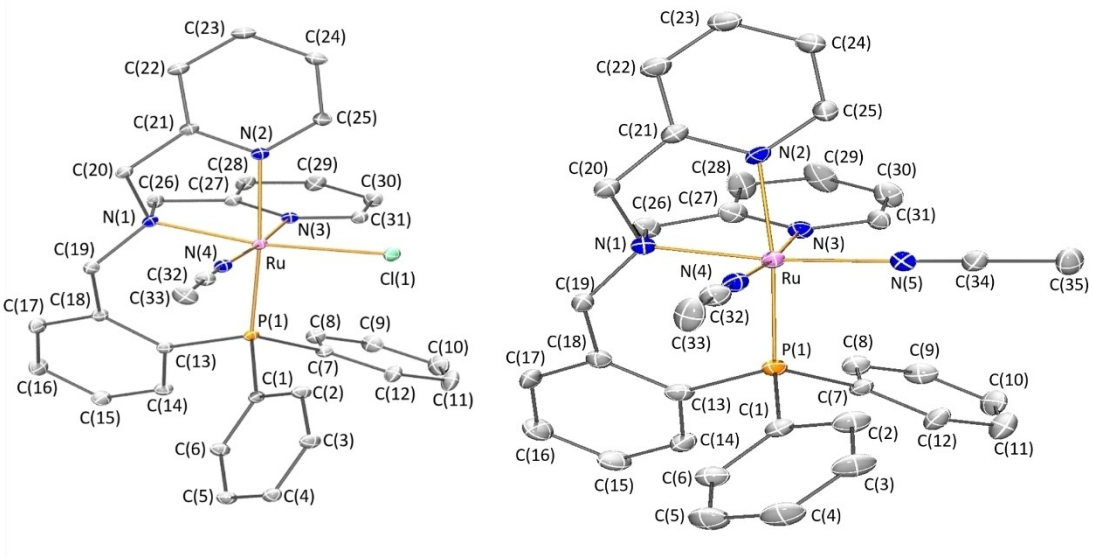

Figure 3. Structures of the cations of **4** (left) and **5**·$(CH_2Cl_2)_{0.25}$ (right). For clarity, hydrogen atoms and partial solvate molecule have been omitted.

Table 2. Selected bond lengths (Å) and angles (°) for complexes **4** and **5**·$(CH_2Cl_2)_{0.25}$.

	4	**5**[b]		**4**	**5**[b]
Ru–X[a]	2.4169(4)	2.041(7)	P(1)–Ru–N(1)	94.12(4)	93.53(18)
Ru–P(1)	2.2760(4)	2.275(2)	P(1)–Ru–N(2)	172.13(4)	172.76(18)
Ru–N(1)	2.1020(13)	2.104(7)	P(1)–Ru–N(3)	89.51(4)	93.34(19)
Ru–N(2)	2.1285(13)	2.128(6)	P(1)–Ru–N(4)	93.74(4)	91.78(19)
Ru–N(3)	2.0493(13)	2.042(6)	N(1)–Ru–N(2)	79.94(5)	79.8(2)
Ru–N(4)	2.0276(14)	2.046(7)	N(1)–Ru–N(3)	82.65(5)	82.6(3)
X[a]–Ru–P(1)	94.702(13)	93.06(19)	N(1)–Ru–N(4)	94.20(5)	93.7(3)
X[a]–Ru–N(1)	170.76(4)	173.2(3)	N(2)–Ru–N(3)	84.63(5)	83.1(3)
X[a]–Ru–N(2)	91.02(4)	93.5(3)	N(2)–Ru–N(4)	91.86(5)	91.4(3)
X[a]–Ru–N(3)	94.68(4)	95.3(3)	N(3)–Ru–N(4)	175.64(5)	173.8(3)
X[a]–Ru–N(4)	87.96(4)	87.8(3)			

[a] X=Cl(1) for **4** and N(4) for **5**. [b] Asymmetric unit of **5** contains two cations and geometric parameters of one are reported here. Full information may be found in Supporting Information.

Consistent with the NMR spectroscopic data, the coordinated acetonitrile is *trans* to the pyridinic N(3). Simultaneously, the chlorine atom Cl(1) is *trans* to N(1). The Ru–Cl(1) bond length (2.4169(4) Å) in **4** is slightly shorter than the Ru–Cl(1) bond in **2** (2.4341(3) Å), likely due to the increased formal charge on the metal centre. Reflecting different *trans* influence, the Ru–N(2) bond distance (2.1285(13) Å, *trans* to the P(1) atom) is approximately 0.0792 Å longer than the Ru–N(3) bond distance (2.0493(13) Å, *trans* to the acetonitrile group. Based on the arrangement of the coordination atoms around the metal, **4** is a chiral-at-ruthenium complex, identified as the *OC*-6-54 diastereomer.

In conclusion, the study of dichlorido compounds **1** and **2** in the presence of one equivalent of $AgSbF_6$ has revealed a marked asymmetry in the reactivity of the two chloride ligands. This well-differentiated behaviour leads to the selective abstraction of one chloride ligand. This process takes place more easily for the ruthenium complex than for the rhodium complex and, in both cases, complete diastereoselectivity towards the chiral-at-metal isomer *OC*-6-54 was achieved. Notably, the relative configuration at metal in **3** and **4** remains unchanged when one acetonitrile molecule replaces one chloride ligand.

Synthesis and Characterization of Complex [Ru(κ^4-$N_2N'P$-L)$(NCMe)_2$][SbF_6]$_2$ (5)

After the characterisation of monoacetonitrile complexes **3** and **4**, attempts were made to replace the second chloride ligand with another acetonitrile molecule. Two methods were used to obtain the diacetonitrile complexes [M(κ^4-$N_2N'P$-L)$(NCMe)_2$][SbF_6]$_n$ (M=Rh, n = +3; Ru, n = +2) (Scheme 6). The first method involved the abstraction of both chlorides by adding 2 equiv. of $AgSbF_6$ to the dichlorido complexes **1** and **2**.

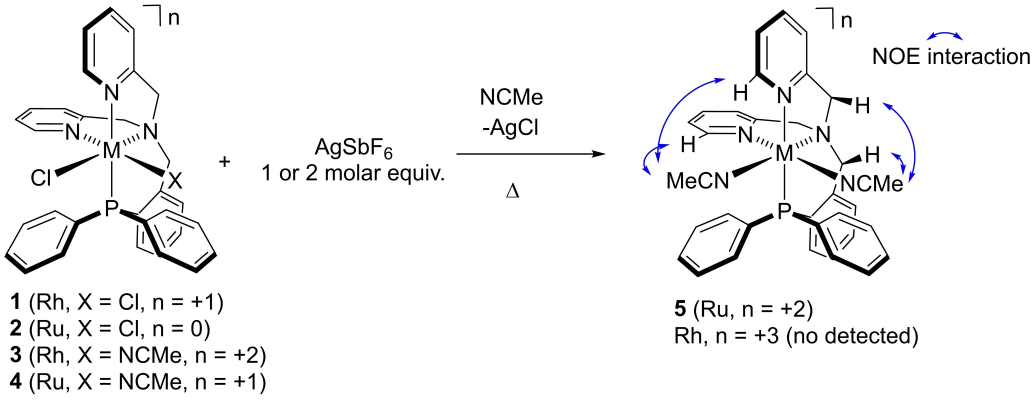

Scheme 6. Synthesis of bisacetonitrile complex **5** and NOE interactions.

The second method used a similar approach but started from the monochlorido complexes **3** and **4**.

Treatment of the rhodium complexes **1** and **3** with $AgSbF_6$ at 70 °C for several days did not lead to abstraction of the second chloride ligand. This is probably due to the high Lewis acidity of the Rh(III) centre in trivalent cationic compounds with this type of ligand, which inhibits the substitution of the second chloride ligand. However, in the case of ruthenium complexes **2** and **4**, both methods yielded the complex [Ru(κ^4-$N_2N'P$-**L**)(NCMe)$_2$][SbF_6]$_2$ (**5**).

Treatment of **2** and **4** with $AgSbF_6$ at 60 °C for 12 h resulted in the formation of complex **5** with a yield of 83 %. Complex **5** was characterised by analytical and spectroscopic methods (see Experimental Section) and X-ray diffraction studies (Figure 3, Table 2). The NMR data for complex **5** enabled the assignment of the six different methylenic protons of the coordinated ligand **L** and the protons 6-CH(Py_{cisP}) (8.74 ppm, pt, J = 5.6 Hz) and 6-CH(Py_{transP}) (7.89 ppm, m), indicating that the metal centre is stereogenic. The NOESY spectra show interactions between the methyl group of one acetonitrile molecule coordinated (2.63 ppm) with 6-CH(Py_{cisP}) and 6-CH(Py_{transP}), allowing us to assign the signal to the NCMe *trans* to sp^3-N, and the resonance at 1.95 ppm to the NCMe *trans* to pyridine group (Scheme 6). On the other hand, the ^{1}H-^{31}P HMBC experiment shows correlations between the phosphorus atom (50.46 ppm, s) and both coordinated NCMe ligands (see Experimental Section). All NMR spectroscopic data are consistent with completely diastereoselective synthesis of the chiral-at-ruthenium isomer *OC*-6-35 of **5**, which has the same environment as complexes **2** and **4**, except that the chloride ligands have now been replaced by an NCMe molecule.

The cation of complex **5** (Figure 3, Table 2) has a stereogenic ruthenium centre with four ligating atoms of **L** (κ^4-$N_2N'P$) coordinated in a tripodal fashion and two acetonitrile ligands occupying the remaining coordination sites. The phosphorus atom is *trans* to the pyridinic nitrogen N(2), while the nitrile nitrogens N(5) and N(4) are *trans* to the sp^3-N(1) and pyridinic N(3), respectively. The structural data for complex **5** are similar to those obtained for complex **4** and agree well with the spectroscopic data: the *OC*-6-35 isomer of complex **5** is formed and isolated in a completely diastereoselective manner. It is important to note that both acetonitrile complexes, **4** and **5**, have potential as catalysts and could be used as enantioselective catalysts after resolution.

Synthesis and Characterization of Polymetallic Complexes [{RhCl$_2$(κ^4-$N_2N'P$-**L**)}$_2$(μ-Ag)$_2$][SbF_6]$_4$ (**6**) and [{Rh(κ^4-$N_2N'P$-**L**)}{Rh(COD)}(μ-Cl)$_2$][SbF_6]$_2$ (**7**)

Due to the challenges associated with the chloride abstraction from the octahedral rhodium(III) complexes **1** and **3**, we decided to explore the potential application of rhodium complex **1** as a ligand, through its two chlorides, for the synthesis of polymetallic complexes. To evaluate this approach, we studied the reaction of [RhCl$_2$(κ^4-$N_2N'P$-**L**)][SbF_6] (**1**) with an equivalent amount of $AgSbF_6$ and [Rh(COD)(NCMe)$_2$][SbF_6] (COD = cyclooctadiene).

At room temperature, a suspension of complex [RhCl$_2$(κ^4-$N_2N'P$-**L**)][SbF_6] (**1**) in acetone reacted with $AgSbF_6$ in a 1:1 molar ratio to give the polymetallic compound [{RhCl$_2$(κ^4-$N_2N'P$-**L**)}$_2$(μ-Ag)$_2$][SbF_6]$_4$ (**6**) (Scheme 7). Complex **6** was isolated as a microcrystalline solid from a concentrated solution in dichloromethane with a yield of 80 %. Complex **6** was characterised by analytical and spectroscopic methods (see Experimental Section) and X-ray diffraction studies (Figure 4, Table 3). The structure of the polymetallic cation consists of two octahedral {RhCl$_2$(κ^4-$N_2N'P$-**L**)} fragments coordinated to two silver atoms through the two chloride atoms. An inversion centre relates both octahedral fragments, and therefore the polynuclear complex contains two rhodium centres with opposite absolute configurations.

The rhodium-chloride bonds are similar, with bond lengths of Rh–Cl(1) at 2.3680(7) Å and Rh–Cl(2) at 2.3583(7) Å. The silver-chloride bond distances are also comparable, with Ag–Cl(1) at 2.6107(8) Å and Ag–Cl(2) at 2.5826(8) Å.[20] To the best of our knowledge, there are very few examples of Cl_2Ag bridging complexes.[20,21] In particular, the related complex [{Rh(κ^4-*C,N,N',P*)(NCMe)(μ-Cl)}$_2$Ag][SbF_6]$_3$ (*C,N,N',P* = tripodal tetradentate monoanionic ligand)[21a] has a significantly shorter Ag–Cl bond length (2.5360(15) Å) and a Cl–Ag–Cl angle of 120.19(8)°,

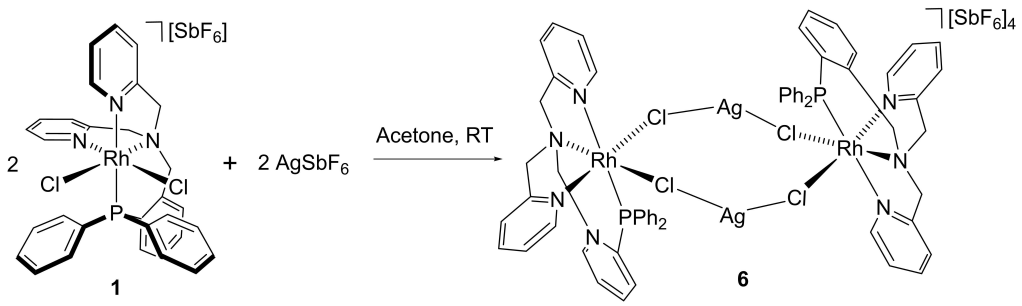

Scheme 7. Synthesis of polymetallic complex **6**.

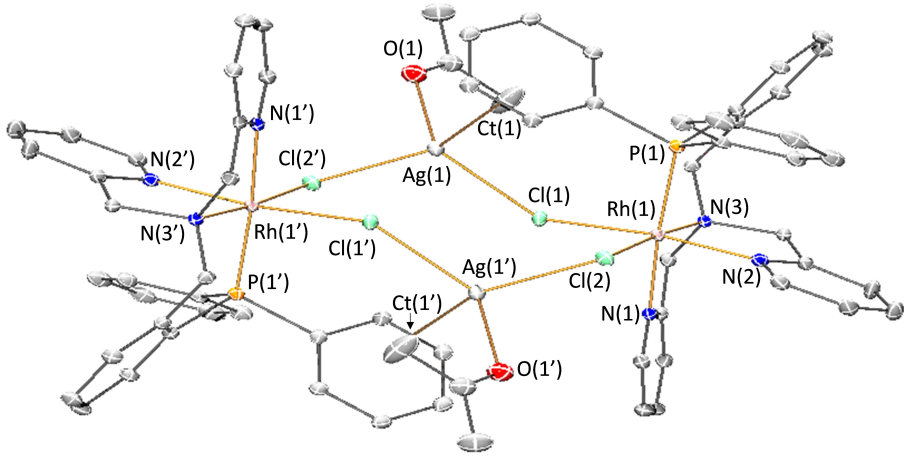

Figure 4. Structure of the cation of **6**·$((CH_3)_2CO)_2$. For clarity, hydrogen atoms have been omitted. Symmetry operation: ′) 1-*x*, 2-*y*, 2-*z*. Ct is the centroid of the C=C bond of the phenyl ring, interacting with Ag.

Table 3. Selected bond lengths (Å) and angles (°) for complex **6**·$((CH_3)_2CO)_2$.

Rh(1)–Cl(1)	2.3680(7)	Cl(2)–Rh(1)–P(1)	89.94(3)
Rh(1)–Cl(2)	2.3583(7)	Cl(2)–Rh(1)–N(1)	95.25(7)
Rh(1)–P(1)	2.2933(8)	Cl(2)–Rh(1)–N(2)	93.99(7)
Rh(1)–N(1)	2.120(2)	Cl(2)–Rh(1)–N(3)	175.43(7)
Rh(1)–N(2)	2.026(2)	P(1)–Rh(1)–N(1)	174.38(7)
Rh(1)–N(3)	2.068(2)	P(1)–Rh(1)–N(2)	93.76(7)
Cl(1)–Rh(1)–Cl(2)	88.86(3)	P(1)–Rh(1)–N(3)	94.37(7)
Cl(1)–Rh(1)–P(1)	95.52(3)	N(1)–Rh(1)–N(2)	83.75(10)
Cl(1)–Rh(1)–N(1)	86.75(7)	N(1)–Rh(1)–N(3)	80.39(10)
Cl(1)–Rh(1)–N(2)	170.29(7)	N(2)–Rh(1)–N(3)	84.21(10)
Cl(1)–Rh(1)–N(3)	92.24(7)	Cl(1)–Ag(1)–O(1)	119.93(7)
Ag(1)–Cl(1)	2.6107(8)	Cl(1)–Ag(1)–Ct(1)	95.47(7)
Ag(1)–Cl(2′)	2.5826(8)	Cl(2′)–Ag(1)–O(1)	84.22(7)
Ag(1)–O(1)	2.430(3)	Cl(2′)–Ag(1)–Ct(1)	144.03(9)
Ag(1)–Ct(1)	2.510(4)	O(1)–Ag(1)–Ct(1)	103.13(10)
Cl(1)–Ag(1)–Cl(2′)	111.42(2)		
Rh(1)···Rh(1′)	7.4411(5)	Rh(1)···Ag(1)	4.5791(4)
Ag(1)···Ag(1′)	3.9162(3)	Rh(1)···Ag(1′)	3.7928(4)

which is much larger than that found for complex **6** (111.42(2)°).

Intriguingly, the silver atoms interact with two carbon atoms from the aromatic rings of the phosphane groups (Ag···Ct(C=C), 2.510(4) Å, Ct=centroid),[22] with an acetone molecule and two diastereotopic chloride ligands (chloride *trans* to pyridine and chloride *trans* to sp^3-N), resulting in a distorted tetrahedral geometry around the silver centres. This arrangement creates a stereogenic environment around the silver atoms. Considering the priority rules[15] Cl(2′) > Cl(1) > Ct(C=C) > O(1) for Ag(1) and Cl(2) > Cl(1′) > Ct(C=C) > O(2) for Ag(1′), Ag(1) has the *S* configuration and Ag(1′) has the *R* configuration. Additionally, within each dichlorido fragment {$RhCl_2(\kappa^4$-$N_2N'P$-**L**)}, the two stereogenic rhodium centres in **6** adopt different absolute configurations (shown in Figure 4): anti-clockwise and clockwise for Rh(1′) and Rh(1), respectively.

The structure of **6** shows that of all the possible diastereomers that can be formed, only one diastereomer crystallises. Therefore, the reaction between the dichloride complex **1** and $AgSbF_6$ to give the tetranuclear compound **6** (see Scheme 7) proceeds with chiral molecular self-recognition: only tetrametallic cation with the absolute configuration $A_{Rh(1')}$,$S_{Ag(1)}$,$R_{Ag(1')}$,$C_{Rh(1)}$-**6** or $C_{Rh(1')}$,$R_{Ag(1)}$,$S_{Ag(1')}$,$A_{Rh(1)}$-**6** is formed. The origin of this chiral molecular self-recognition is most likely due to the attractive Ag···Ct(C=C) interactions that stabilise the observed diastereomer.

NMR spectra of **6** in acetone-d_6 show only a single set of signals consistent with the tetrametallic species. However, the ^{1}H NMR spectrum, although some signals appear at different chemical shifts, resembles that of complex **1** (Figure 5). Therefore, to investigate whether complex **6** retains its polymetallic structure in solution, we evaluated the hydrodynamic radii (r_H) and diffusion coefficients (D_t) in acetone solutions for complexes **1** and **6** using DOSY experiments. The translational self-diffusion coefficients (D_t, Table 4) are 9.44 m^2/s for **1** and 11.17 m^2/s for **6**, indicating that the polymetallic complex **6** diffuses more slowly than the monomer **1**. The ratio $(D_t)_6/(D_t)_1$ is 1.18, which is close to the ideal calculated value of 1.26[23] for diffusing species with twice the volume of the other. Accordingly, the hydrodynamic radii for complexes **1** and **6** (r_H, Table 4) are 6.0 Å and 7.1 Å, respectively. In summary, the diffusion experiments suggest a tetrametallic structure for complex **6** in acetone solution, although it may also coexist in fast equilibrium with other related species of lower nuclearity (Scheme 8).

Table 4. Diffusion coefficient (D_t, m^2s^{-1}), hydrodynamic radius (r_H, Å) for compounds **1** and **6**.

Comp.	10^{10} D_t	r_H
1	10.78	4.71
6	7.986	6.36

Conditions: acetone-d_6, 293 K, 22.72×10^{-3} mM. Solvent viscosity: 0.32 cP at 293 K.

Synthesis and Characterization of Intermediate [{Rh(κ^4-$N_2N'P$-L)}{Rh(COD)}(μ-Cl)$_2$][SbF_6]$_2$ (7)

Following the same strategy regarding the possibility of complex [$RhCl_2$(κ^4-$N_2N'P$-**L**)][SbF_6] (**1**) acting as a ligand through its chloride atoms, we investigated this behaviour using metal fragments that form more stable metal-chloride bonds, such as rhodium-chloride bonds in rhodium(I) species. To test this hypothesis, the dichloride complex **1** was reacted with the Rh(I) complex [Rh(COD)$(NCMe)_2$][SbF_6] in a 1:1 molar ratio (Scheme 9). After 40 min of treatment in dichloromethane at room temperature, solids with the formulation [{Rh(κ^4-$N_2N'P$-**L**)}

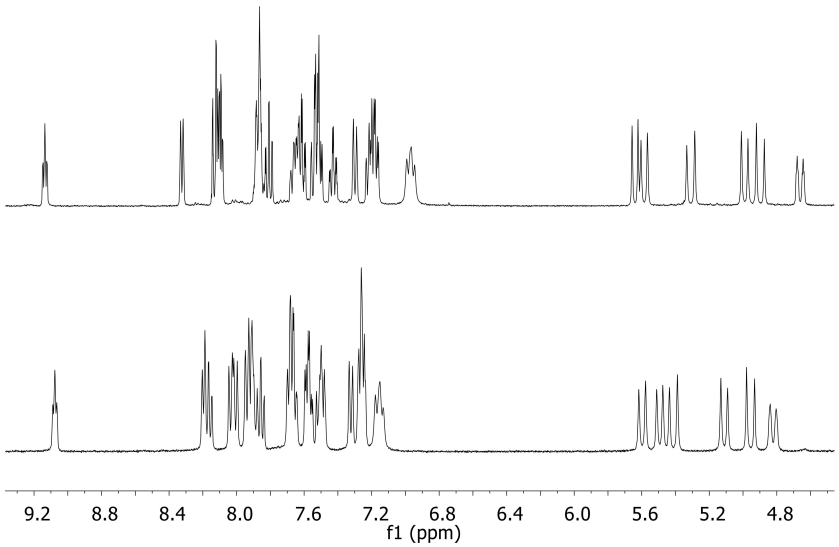

Figure 5. ^{1}H NMR spectra of complexes **1** (up) and **6** (down).

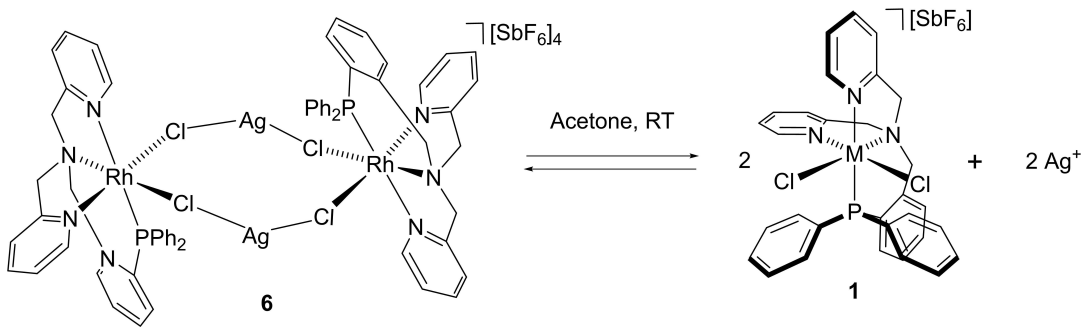

Scheme 8. Possible equilibrium for complex **6** in solution.

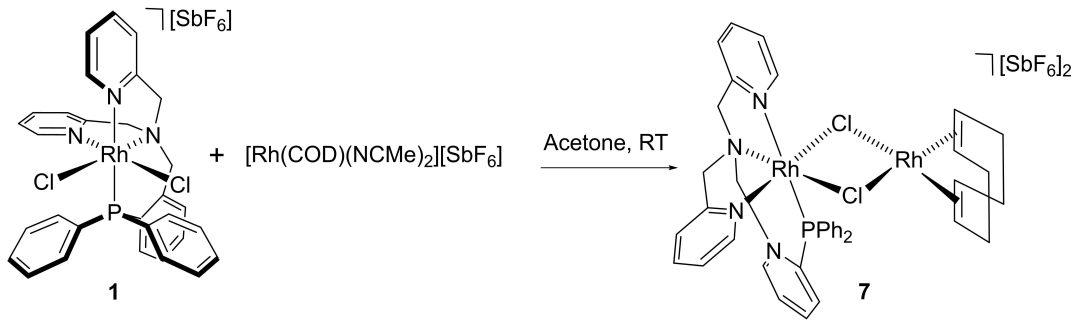

Scheme 9. Synthesis of bimetallic mixed-valence Rh(III)/Rh(I) complex **7**.

{Rh(COD)}(μ-Cl)$_2$][SbF$_6$]$_2$ (**7**) were isolated from the reaction mixture (64%).

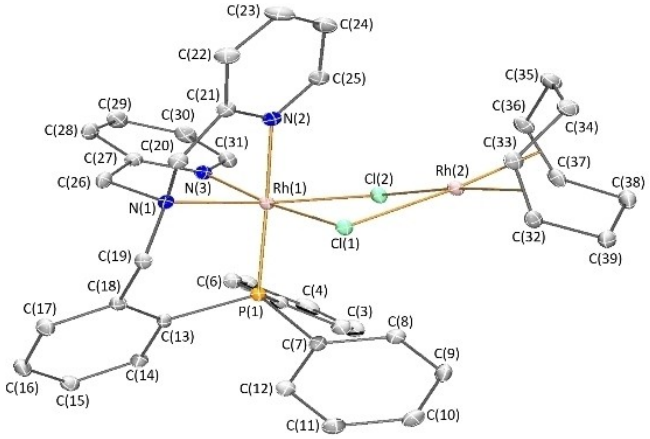

Figure 6. Structure of the cation of **7**·**(CH$_2$Cl$_2$)$_2$**. For clarity, hydrogen atoms and solvate molecules have been omitted.

Table 5. Selected bond lengths (Å) and angles (°) for complex **7**·**(CH$_2$Cl$_2$)$_2$**.

Rh(1)–Cl(1)	2.3693(7)	Cl(2)–Rh(1)–N(1)	174.90(7)
Rh(1)–Cl(2)	2.3787(7)	Cl(2)–Rh(1)–N(2)	94.17(7)
Rh(1)–P(1)	2.3026(7)	Cl(2)–Rh(1)–N(3)	95.67(7)
Rh(1)–N(1)	2.058(2)	P(1)–Rh(1)–N(1)	95.65(6)
Rh(1)–N(2)	2.107(2)	P(1)–Rh(1)–N(2)	175.11(7)
Rh(1)–N(3)	2.024(2)	P(1)–Rh(1)–N(3)	95.93(7)
Rh(2)–Cl(1)	2.4105(7)	N(1)–Rh(1)–N(2)	80.75(9)
Rh(2)–Cl(2)	2.4100(7)	N(1)–Rh(1)–N(3)	83.70(9)
Rh(2)–Ct(1)[a]	1.9796(3)	N(2)–Rh(1)–N(3)	87.00(9)
Rh(2)–Ct(2)[a]	1.9789(3)	Cl(1)–Rh(2)–Cl(2)	84.70(2)
Cl(1)–Rh(1)–Cl(2)	86.31(2)	Cl(1)–Rh(2)–Ct(1)	93.045(18)
Cl(1)–Rh(1)–P(1)	92.05(2)	Cl(1)–Rh(2)–Ct(2)	175.61(2)
Cl(1)–Rh(1)–N(1)	93.62(6)	Cl(2)–Rh(2)–Ct(1)	174.63(2)
Cl(1)–Rh(1)–N(2)	84.92(6)	Cl(2)–Rh(2)–Ct(2)	1.9885(3)
Cl(1)–Rh(1)–N(3)	171.80(7)	Ct(1)–Rh(2)–Ct(2)	88.508(11)
Cl(2)–Rh(1)–P(1)	89.45(3)	Rh(1)···Rh(2)	3.4351(4)

[a] Ct(1) and Ct(2) are the centroid of the C(32)=C(33) and C(36)=C(37) olefinic bonds, respectively.

Single crystals suitable for X-ray diffraction analysis were obtained from dichloromethane solutions of **7** (Figure 6). Table 5 summarises the main parameters of the coordination sphere. The molecular structure of the dicationic complex **7** contains two metal fragments, {Rh(κ^4-*N$_2$N′P*-**L**)} and {Rh(COD)}, linked by two bridging chloride atoms (Figure 6). Mixed-valence Rh(III)/Rh(I) complexes are rare and only a few examples have been reported.[24] The bridging chlorides have similar bond lengths with rhodium(III) (Rh(1)–Cl(1), 2.3692(7) Å; Rh(1)–Cl(2), 2.3784(8) Å) and significantly longer bond lengths with rhodium(I) (Rh(2)–Cl(1), 2.4107(7) Å; Rh(2)–Cl(2), 2.4101(7) Å). These differences reflect greater bond stability between the {Rh(κ^4-*N$_2$N′P*-**L**)} fragment and the bridging chlorides, especially when compared to an unstable mixed-valence complex [{Rh(ppy)$_2$}{Rh(COD)}(μ-Cl)$_2$] (ppy = 2-phenylpyridine anion).[24a] In these complex the Rh(III)–Cl bond distances (2.553(1) and 2.569(2) Å) are much longer, whereas the Rh(I)–Cl bond distances (2.407(1) and 2.410(2) Å) are similar.

When the dinuclear complex **7** was analysed in a dichloromethane solution, the NMR spectroscopic results showed only one set of signals consistent with a bimetallic species in solution. Furthermore, the signal set for complex **7** showed no similarity to that of the mononuclear dichlorido complex **1** or the complex [Rh(COD)(NCMe)$_2$][SbF$_6$]. It can be concluded that the bimetallic complex **7** remains stable both in solution (even after heating 24 h at 60 °C) and in solid state. This suggests that complex **1**, through its two chlorine atoms, can act as a chelating ligand, coordinating to an {Rh(COD)} fragment to form a bimetallic mixed-valence Rh(III)/Rh(I) complex **7** with potential as a catalyst.

Conclusions

Ligand **L** forms tetracoordinated dichlorido complexes with d^6 Rh^{3+} and Ru^{2+} ions, with the general formulae [MCl$_2$(κ^4-*N$_2$N′P*-**L**)]^n (M=Rh, n = +1; Ru, n = 0), showing complete diastereoselectivity. Specifically, for the dichlorido complexes **1** and **2**, a unique chiral *OC*-6-43 isomer is formed in which the two pyridine groups are in *cis* disposition.

In a highly stereoselective manner, only the chloride ligand in *trans* to pyridine can be abstracted by adding one equivalent of AgSbF$_6$. While the abstraction of chloride from rhodium

complex **1** requires elevated temperatures and prolonged reaction times, the reaction with ruthenium complex **2** takes place at room temperature and in shorter times. These differences highlight the different behaviour of the d^6 Rh^{3+} and Ru^{2+} ions concerning the lability of the chloride ligand, which is influenced by the formal charge and Lewis acidity of the metal centre.

Under the reaction conditions used, the abstraction of the second chloride ligand does not occur in rhodium complexes **1** and **3**. However, for ruthenium, treatment of complexes **2** and **4** with the appropriate amount of $AgSbF_6$ gives the bisacetonitrile chiral-at-metal complex $[Ru(\kappa^4\text{-}N_2N'P\text{-}\mathbf{L})(NCMe)_2][SbF_6]_2$ (**5**).

The reluctance of complex **1** to substitute chloride ligands led us to explore its use as a ligand through the chlorine atoms in Ag(I) and Rh(I) complexes. The resulting silver complex **6** is a tetrametallic species with two Ag centres and two octahedral units of the $\{RhCl_2(\kappa^4\text{-}N_2N'P\text{-}\mathbf{L})\}$ fragment coordinated to each silver atom through the chlorides. This polymetallic complex has four stereogenic metal centres and is obtained with complete diastereoselectivity by chiral molecular self-recognition. The stabilising Ag···Ct(C=C) interactions probably explain the preferential formation of the isolated isomer. According to DOSY NMR data, complex **6** seems to retain its polymetallic nature in solution. However, a possible equilibrium between the tetrametallic species and other species of lower nuclearity cannot be ruled out. The use of the $\{RuCl_2(\kappa^4\text{-}N_2N'P\text{-}\mathbf{L})\}$ fragment as a ligand was also demonstrated by the formation of the complex $[\{Rh(\kappa^4\text{-}N_2N'P\text{-}\mathbf{L})\}\{Rh(COD)\}(\mu\text{-}Cl)_2][SbF_6]_2$ (**7**), whose bimetallic structure remains stable in solution.

Upon resolution of the chiral-at-metal complexes, complexes **1–2** could show great potential as enantioselective precatalysts, with complex **1** also working as a chiral ligand. We are currently pursuing these lines of research in our laboratory.

Experimental Section

General Information

All preparations have been carried out under argon. All solvents were treated in a PS-400-6 Innovative Technologies Solvent Purification System (SPS) and degassed before use. Carbon, hydrogen and nitrogen analyses were performed using a Perkin-Elmer 240 B microanalyser. ^1H, ^{13}C and ^{31}P and spectra were recorded on a Bruker AV-300, a Bruker AV-400 or a Bruker AV-500 spectrometers. Chemical shifts are expressed in ppm downfield from $SiMe_4$ or 85% H_3PO_4 (^{31}P). COSY, NOESY, HSQC, HMQC, and HMBC ^1H–X (X=^1H, ^{13}C, ^{31}P) correlation spectra were obtained using standard procedures. The protons have been assigned according to the enantiomer drawn. DOSY experiments were carried out using the PFGSE (pulsed-field gradient spin-echo) NMR Diffusion methods and analysed with the software implemented by Bruker on an NMR AV500 spectrometer. Hydrodynamic radii (r_H) were calculated from the Stokes-Einstein equation: $r_H = kT/6\pi\eta D_t$ where T is the absolute temperature, k is the Boltzmann constant, η is the solvent viscosity and D_t is the translational self-diffusion coefficient. Infrared spectra were recorded on a Perkin-Elmer Spectrum One FT IR spectrophotometer. Mass spectra were obtained with a Micro Tof-Q Bruker Daltonics spectrometer. Di-(2-picoliyl)amine (99%) and 2-diphenylphosphinobenzaldehyde (97%) were purchased from Fluorochem and Pharmatech respectively and were used without further purification.

Preparation and Characterisation of $N_2N'P$ ligand

To a solution of di-(2-picoliyl)amine 2.06 g (10.33 mmol) in 20 mL of CH_2Cl_2, 3.00 g (10.33 mmol) of 2-diphenylphosphinobenzaldehyde and 3.35 g (15.81 mmol) of $NaBH(AcO)_3$ were added. The resulting solution was stirred for 24 h at room temperature and then 50 mL of a saturated solution of $NaHCO_3$ in water was added. After 15 min of additional stirring the organic phase was separated by decantation, washed with water (3×75 mL) and dried ($MgSO_4$). The insoluble materials were removed by filtration and all volatiles were removed under vacuum. The addition of 15 mL of n-pentane to the oily residue affords the ligand as an analytical pure solid compound. Yield: 4.37 g (9.23 mmol, 89%). Anal. calc. for $C_{31}H_{28}N_3P$: C, 78.63; H, 5.96; N, 8.87. Found: C, 78.71; H, 6.18; N, 8.62. HRMS (μ-TOF): $C_{31}H_{28}N_3P$, $[M+H]^+$: calc. 474.2094, found 474.2089. The NMR data are in good agreement with those found in the literature.[14]

[RhCl$_2$(κ^4-N$_2$N'P-L)][SbF$_6$] (1)

To a suspension of $RhCl_3\ xH_2O$ (500.0 mg, 1.92 mmol) in 40 mL ethanol 909.2 mg (1.92 mmol) of **L** and 500.0 mg (1.93 mmol) of $NaSbF_6$ were added. The resulting suspension was stirred overnight under reflux. During this time, the pink-red suspension became yellow. The suspension was vacuum-dried and extracted with dichloromethane. The resulting yellow solution was vacuum-dried to give a microcrystalline yellow solid. Yield: 1249.9 mg (1.42 mmol, 74%). Crystals suitable for X-ray diffraction analysis were obtained by crystallisation from CH_2Cl_2/Et_2O solution at RT. Anal. calc. for $C_{31}H_{28}Cl_2F_6N_3PRhSb$: C, 42.16; H, 3.20; N, 4.76. Found: C, 42.39; H, 3.34; N, 4.63. IR ν(SbF_6) 653 (s) (solid, cm^{-1}). HRMS (μ-TOF): $C_{31}H_{28}Cl_2F_6N_3PRhSb$, $[M\text{-}SbF_6]^+$ calc. 646.0447, found 646.0442. *^1H NMR (400.16 MHz, CD_2Cl_2, RT, ppm):* $\delta = 9.11$ (pseudo-triplet, J = 4.1 Hz, 1H, 6-CH(Py_{transP})), 8.29 (d, J = 5.7 Hz, 1H, 6-CH(Py_{cisP})), 8.13-7.95 (m, 3H, CH_{Ar}), 7.81 (br, 3H, CH_{Ar}), 7.73 (pseudo-triplet, J = 7.0 Hz, 1H, CH_{Ar}), 7.21 (d, J = 7.8, 1.3 Hz, 1H, 3-CH(Py_{cisP})), 7.13 (ddd, J = 15.1, 9.6, 5.2 Hz, 3H, 2×CH_{Ar}, 5-CH(Py_{cisP})), 6.92 (m, 2H, CH_{Ar}), 5.60 (d, J = 14.0 Hz, 1H, *pro-S*-CH_2(P)), 5.53 (d, J = 15.53 Hz, 1H, *pro-R*-CH_2(Py_{transP})), 5.15 (d, J = 18.8 Hz, 1H, *pro-R*-CH_2(Py_{cisP})), 4.89 (d, J = 15.3 Hz, 1H, *pro-R*-CH_2(Py_{transP})), 4.75 (d, J = 18.8 Hz, 1H, *pro-S*-CH_2(Py_{cisP})), and 4.54 (d, J = 13.9 Hz, 1H, *pro-R*-CH_2(P)). *$^{13}C\{^1H\}$ NMR (100.62 MHz, CD_2Cl_2, RT, ppm):* $\delta = 162.9$ (s, 2-C(Py_{transP})), 157.03 (s, 2-CH(Py_{transP})), 150.31 (s, 6-CH(Py_{cisP})), 148.53 (s, 6-CH(Py_{transP})), 141.82-121.91 (m, 24 CH_{Ar}), 75.35 (s, CH_2(Py_{transP}), 67.89 (s, CH_2(Py_{cisP}), and 66.28 (d, J = 4.9 Hz, CH_2(P). *$^{31}P\{^1H\}$ NMR (161.98 MHz, CD_2Cl_2, RT, ppm):* $\delta = 30.66$ (d, J = 107.6 Hz).

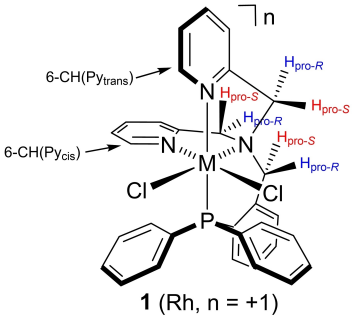

1 (Rh, n = +1)
2 (Ru, n = 0)

[RuCl$_2$(κ^4-N$_2$N'P-L)] (2)

To a suspension of {(η^6-C$_6$H$_6$)RuCl}$_2$(μ-Cl)$_2$ (250.0 mg, 0.50 mmol) in 40 mL ethanol, 473.0 mg (1.00 mmol) of **L** was added. The resulting suspension was stirred overnight under reflux. The resulting yellow solution was vacuum-dried to give the compound **2**. Recrystallisation from CH_2Cl_2/Et_2O gives a microcrystalline yellow solid. Crystals suitable for X-ray diffraction analysis were obtained by crystallisation from CH_2Cl_2/Et_2O solution at RT. Yield: 582.0 mg (0.902 mmol, 90%). Anal. calc. for $C_{31}H_{28}Cl_2N_3PRu$: C, 57.68; H, 4.37; N, 6.51. Found: C, 56.86; H, 4.21; N, 6.42. HRMS (μ-TOF): $C_{31}H_{28}Cl_2N_3PRu$, $[M+H]^+$ calc. 646.0516, found 646.0513. *^{1}H NMR (300.13 MHz, CD_2Cl_2, RT, ppm):* δ = 9.62 (t, *J* = 2.0 Hz, 1H, 6-CH(Py_{transP})), 8.53 (d, *J* = 4.7 Hz, 1H, 6-CH(Py_{cisP})), 8.20 (m, 2H, CH(Ar)), 7.68 (td, *J* = 7.6, 1.6 Hz, 1H, 4-CH(Py_{transP})), 7.54 (m, 2H, CH(Ar)), 7.48-7.34 (m, 6H, 5×CH(Ar), 3-CH (Py_{transP})), 7.25 (t, *J* = 7.0 Hz, 1H, 5-CH(Py_{transP})), 7.13 (td, *J* = 7.8, 1.5 Hz, 1H, 4-CH(Py_{cisP})), 7.10 (td, *J* = 7.8, 1.5 Hz, 1H, CH(Ar),) 6.99 (td, *J* = 7.2, 2.0 Hz, 2H, CH(Ar)), 6.73 (t, *J* = 8.7 Hz, 2H, CH(Ar)), 6.59(d, *J* = 7.7 Hz, 1H, 3-CH (Py_{cisP})), 6.54 (d, *J* = 7.7 Hz, 1H, 5-CH(Py_{cisP})), 5.63 (d, *J* = 14.0 Hz, 1H, CH_2(*pro-S*-P)), 5.27 (d, *J* = 15.3 Hz, 1H, CH_2(*pro-R*-Py_{transP})), 4.23 (d, *J* = 18.8 Hz, 1H, CH_2(*pro-S*-Py_{cisP})), 4.09 (d, *J* = 14.9 Hz, 1H, CH_2(*pro-S*-Py_{transP})), 4.03 (d, *J* = 14.1 Hz, 1H, CH_2(*pro-R*-P)), 6.69 (d, *J* = 18.4 Hz, 1H, CH_2(*pro-R*-Py_{cisP})). *^{13}C{^{1}H} NMR (100.62 MHz, CD_2Cl_2, RT, ppm):* δ = 162.90 (s, 2-C(Py_{cisP})), 157.03 (d, *J* = 2.5 Hz, 2-C(Py_{transP})), 150.31 (s, 6-CH(Py_{cisP})), 148.53 (s, 6-CH(Py_{transP})), 141.82-121.91 (m, 24 C(Ar)), 75.35 (s, CH_2(Py_{transP})), 67.89 (s, CH_2(Py_{cisP})), 66.28 (d, *J* = 4.9 Hz, CH_2(P)). *^{31}P{^{1}H} NMR (121.49 MHz, CD_2Cl_2, RT, ppm):* δ = *58.76 (br).*

[RhCl(κ^4-N$_2$N'P-L)(NCMe)][SbF$_6$]$_2$ (3)

To a solution of complex [$RhCl_2$(κ^4-*N$_2$N'P*-**L**)][SbF_6] (**1**) (300.0 mg, 0.340 mmol) in 40 mL acetonitrile 117.2 mg (0.341 mmol) of $AgSbF_6$ were added, and the resulting suspension was stirred for 4 days at 60 °C. The suspension was filtered, and the filtrate was concentrated under reduced pressure to ca. volume of 1 mL. The slow addition of 15 mL of Et_2O led to the precipitation of a yellow solid which was washed with Et_2O (3×5 mL) and vacuum-dried to give an analytical pure compound. Yield: 307.2 mg (0.273 mmol, 80%). Anal. calc. for $C_{33}H_{31}Cl_1F_{12}N_4PRhSb_2$: C, 35.25; H, 2.78; N, 4.98. Found: C, 35.39; H, 2.90; N, 4.80. IR (solid, cm^{-1}): ν(CN) 2308 (br), ν(SbF_6) 650 (s). HRMS (μ-TOF): $C_{33}H_{31}Cl_1F_{12}N_4PRhSb_2$, $[M\text{-}2SbF_6+CH_3O]^+$ calc. 683.1283, found 683.1277.

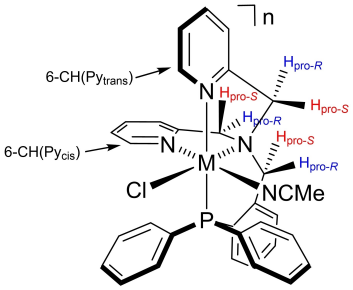

3 (Rh, n = +2)
4 (Ru, n = +1)

^{1}H NMR (500.13 MHz, CD_2Cl_2, RT, ppm): δ = 8.98 (t, *J* = 4.3 Hz, 1H, 6-CH(Py_{transP})), 8.25 (d, *J* = 6.1 Hz, 1H, 6-CH (Py_{cisP})), 8.10 (td, *J* = 7.8, 1.5 Hz, 1H, 4-CH-(Py_{transP})),7.91(m, 6H, 5×CH(Ar), 6-CH (Py_{transP})), 7.80 (td, *J* = 7.8, 1.4 Hz, 1H, 4-CH(Py_{cisP})), 7.76-7.70 (m, 2H, CH(Ar)), 7,65 (m, 4H, CH(Ar)), 7,58 (m, 3H, 2×CH(Ar), 5-CH (Py_{transP})), 7.39 (ddd, *J* = 10.9, 7.9, 1.1 Hz, 1H, CH(Ar)), 7.32-7.34(br, 2H, CH(Ar)), 722 (d, *J* = 7.4 Hz, 1H, 3-CH(Py_{cisP})), 7.16 (t, *J* = 6.8 Hz, 1H, 5-CH(Py_{cisP})), 5.31 (d, *J* = 10.1 Hz, 1H, CH_2(*pro-S*-Py_{transP})), 5.08 (d, *J* = 19.3 Hz, 1H, CH_2(*pro-R*-Py_{cisP})), 4.98 (d, *J* = 14.1 Hz, 1H, CH_2(*pro-S*-P)), 4.95 (d, *J* = 15.8 Hz, 1H, CH_2(*pro-R*-Py_{transP})), 4.71 (d, *J* = 16.3 Hz, 1H, CH_2(*pro-R*-P)), 4.58 (d, *J* = 19.3 Hz, 1H, CH_2(*pro-S*-Py_{cisP})), 1.94 (s, 3H, $NCCH_3$). ^{13}C{^{1}H}NMR (125.77 MHz, CD_2Cl_2, RT, ppm): δ = 163.43 (s, 2-C(Py_{cisP})), 159.63 (s, 2-C(Py_{transP})), 150.53 (s, 6-CH(Py_{cisP})), 148.60 (s, 6-CH(Py_{transP})), 142.44-120.26 (m, 24 C(Ar)), 127.10 (d, *J* = 5.5 Hz, NCMe), 74.74 (s, CH_2(Py_{transP})), 67.83 (d, *J* = 5.8 Hz, CH_2(P)), 65.70 (s, CH_2(Py_{cisP})), 3.85 (s, NC*Me*).

^{31}P{^{1}H} NMR (202.46 MHz, CD_2Cl_2, RT, ppm): δ = 28.80 (d, *J* = 98.2 Hz).

[RuCl(κ^4-N$_2$N'P-L)(NCMe)][SbF$_6$] (4)

To a solution of complex [$RuCl_2$(κ^4-*N$_2$N'P*-**L**)] (**2**) (210.0 mg, 0.325 mmol) in 20 mL acetonitrile 111.8 mg (0.325 mmol) of $AgSbF_6$ were added, and the resulting suspension was stirred for 6 h at RT. The suspension was filtered, and the filtrate was concentrated under reduced pressure to a ca. volume of 1 mL. The slow addition of 10 mL of Et_2O led to the precipitation of a yellow solid which was washed with Et_2O (3×5 mL) and vacuum-dried to give an analytical pure compound. Yield: 258.5 mg (0.291 mmol, 90%). Crystals suitable for X-ray diffraction analysis were obtained by crystallisation from CH_2Cl_2/Et_2O solution at RT. Anal. calc. for $C_{33}H_{31}Cl_1F_6N_4PRuSb$: C, 44.69; H, 3.52; N, 6.32. Found: C, 44.87; H, 3.55; N, 6.33. HRMS (μ-TOF): $C_{33}H_{31}Cl_1F_6N_4PRuSb$, [M-$SbF_6$-NCMe]$^+$: calc. 610.0752, found 610.0753. ^{1}H NMR (300.13 MHz, CD_2Cl_2, RT, ppm): δ = 9.31 (m, 1H, 6-CH(Py_{transP})), 8.68 (d, *J* = 6.1 Hz, 1H, 6-CH (Py_{cisP})), 7.82 (m, 4H, CH(Ar)), 7.66 (m, 2H, CH(Ar)), 7.53 (m, 3H, CH(Ar)), 7.76-7.70 (m, 2H, CH(Ar)), 7,65 (m, 4H, CH(Ar)), 7,58 (m, 3H, CH(Ar)), 7.39 (ddd, *J* = 10.9, 7.9, 1.1 Hz, 1H, CH(Ar)), 7.16 (t, *J* = 6.8 Hz, 1H, CH(Ar)), 5.31 (d, *J* = 10.1 Hz, 1H, CH_2(*pro-S*-Py_{transP})), 5.08 (d, *J* = 19.3 Hz, 1H, CH_2(*pro-R*-Py_{cisP})), 4.98 (d, *J* = 14.1 Hz, 1H, CH_2(*pro-S*-P)), 4.95 (d, *J* = 15.8 Hz, 1H, CH_2(*pro-R*-Py_{transP})), 4.71 (d, *J* = 16.3 Hz, 1H, CH_2(*pro-R*-P)), 4.58 (d, *J* = 19.3 Hz, 1H, CH_2(*pro-S*-Py_{cisP})), 1.85 (s, 3H, $NCCH_3$). ^{13}C{^{1}H} NMR (75.47 MHz, CD_2Cl_2, RT, ppm): δ = 162.60 (s, 2-C(Py_{cisP})), 157.73 (s, 2-C(Py_{transP})), 152.70 (s, 6-CH(Py_{cisP})), 150.17 (s, 6-CH(Py_{transP})), 142.44-120.26 (m, 24 C(Ar)), 126.17 (S, NCMe), 73.87 (s, CH_2(Py_{transP})), 68.56 (d, *J* = 5.3 Hz, CH_2(P)), 64.52 (s, CH_2(Py_{cisP})), 3.73 (s, NC*Me*). ^{31}P{^{1}H} NMR (121.49 MHz, CD_2Cl_2, RT, ppm): δ = 55.58 (s).

[Ru(κ^4-*N$_2$N'P*-L)(NCMe)$_2$][SbF$_6$]$_2$ (5)

To a suspension of [$RuCl_2$(κ^4-*N$_2$N'P*-**L**)] (**2**) (145.6 mg, 0.226 mmol) in 20 mL of NCMe, 157.2 mg (0.457 mmol) of $AgSbF_6$ were added under argon atmosphere. The suspension was left stirring for 12 h at 60 °C and then, the AgCl precipitate was separated by filtration through the cannula. The resulting solution was vacuum-dried to give the compound **5** as an oily residue. The red-orange oily residue was triturated under vigorous stirring with diethyl ether. Then, the orange solid was washed with pentane (3×5 mL) and vacuum-dried to give an analytical pure compound. Yield: 210.5 mg (0.187 mmol, 83%). Crystals suitable for X-ray diffraction analysis were obtained by crystallisation from CH_2Cl_2/Et_2O solution at RT. Anal. calc. for $C_{35}H_{34}F_{12}N_5PRuSb_2$: C, 37.26; H, 3.04; N, 6.21. Found: C, 37.31; H, 3.14; N, 6.09. IR (solid, cm^{-1}): ν(CN) 2308 (br), ν(SbF_6) 650 (s). HRMS (μ-TOF): $C_{35}H_{34}F_{12}N_5PRuSb_2$, [M-2($SbF_6$)-NCMe–H]$^+$: calc. 615.1255, found 615.1249.

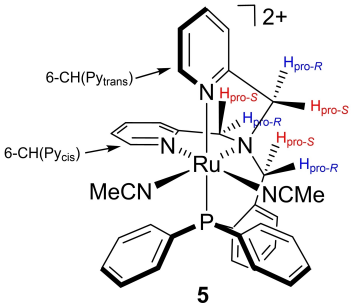

5

^{1}H NMR (500.13 MHz, CD_2Cl_2, RT, ppm) $\delta = 8.74$ (pseudo-triplet, $J =$ 5.6 Hz, 1H, 6-CH(Py$_{transP}$)), 7.89 (m, 2H, 6-CH(Py$_{cisP}$), (CH(Py$_{transP}$)), 7.69 (m, 3H, 4-CH(Py$_{cisP}$), CH(Ar)), 7.59 (m, 3H, CH(Ar)), 7.53 (td, $J = 7.75$, 1.5 Hz, 1H, 4-CH(Py$_{cisP}$)), 7.47 (m, 3H, CH(Py$_{transP}$), CH(Ar)), 7.36 (m, 2H, CH(Ar)), 7.32 (m, 1H, CH(Ar)), 7.27 (m, 2H, CH(Ar)), 7.15 (pseudo-triplet, 1H, $J = 9.6$ Hz, CH(Py$_{transP}$)), 7.12 (t, $J = 6.2$ Hz, 1H, 5-CH(Py$_{cisP}$)), 6.91 (d, $J = 7.8$ Hz, 1H, 3-CH(Py$_{cisP}$)), 6.78 (dd, $J = 7.1$, 1.9 Hz, 2H, CH(Ar)), 4.80 (d, $J = 15.5$ Hz, 1H, *pro-R*-CH_2(Py$_{transP}$)), 4.70 (d, 1H, *pro-S*-CH_2(Py$_{transP}$)), 4.60 (m, 3H, CH_2P, *pro-R*-CH_2(Py$_{cisP}$)), 4.02 (d, $J =$ 18.7 Hz, 1H, *pro-S*-CH_2(Py$_{cisP}$)), 2.63 (s, 3H, NCMe *trans* to N), 1.95 (s, 3H, NCMe *trans* to Py). ^{13}C{^{1}H} NMR (125.77 MHz, CD_2Cl_2, RT, ppm): $\delta = 162.15$ (2-C(Py$_{cisP}$)), 156.72 (br, 2-C(Py$_{transP}$)), 152.07 (6-CH(Py$_{cisP}$)), 150.92 (6-CH(Py$_{transP}$)), 140.49 (d, $J = 18.2$ Hz, C(Ar)), 139.80 (4-CH(Py$_{transP}$)), 138.04 (CH(Ar)), 135.39 (5-CH(Py$_{transP}$)), 134.98 (d, $J =$ 9.3 Hz, CH(Ar)), 134.88 (m, 3-CH(Py$_{transP}$)), 133.53 (d, $J = 1.8$ Hz, C(Ar)), 133.46 (d, $J = 10.1$ Hz, 2 C, CH(Ar)), 132.26 (d, $J = 9.7$ Hz, CH(Ar)), 131.57 (d, $J = 1.7$ Hz, CH(Ar)), 130.77 (d, $J = 6.1$ Hz, 4-CH(Py$_{transP}$)), 130.30 (d, $J = 47.1$ Hz, C(Ar), 129.64 (d, $J = 9.8$ Hz, 2 C, CH(Ar)), 129.21 (d, $J = 9.8$ Hz, 2 C, CH(Ar)), 129.02 (d, $J = 45.4$ Hz, C(Ar)), 128.59 (N*C*Me *trans* to Py), 127.74 (N*C*Me *cis* to Py), 127.07 (d, $J =$ 45.1 Hz, C(Ar)), 126.39 (CH(Ar)), 125.42 (3-CH(Py$_{cisP}$)), 123.62 (4-CH(Py$_{cisP}$)), 120.36 (CH(Ar)), 73.03 (CH_2(Py$_{transP}$)), 67.93 (d, $J = 6.2$ Hz, CH_2(P)), 64.51 (CH_2(Py$_{cisP}$)), 4.15 (NC*Me* *trans* to N), 3.61 (s, NC*Me* *trans* to Py). ^{31}P{^{1}H} NMR (202.46 MHz, CD_2Cl_2, RT, ppm): $\delta = 50.46$ (s).

[{RhCl$_2$(κ^4-N$_2$N'P-L)}$_2$(μ-Ag)$_2$][SbF$_6$]$_4$ (6)

To a solution of complex [$RhCl_2$(κ^4-*N$_2$N'P*-**L**)][SbF_6] (**1**) (100.0 mg, 0.113 mmol) in 10 mL acetone 38.9 mg (0.113 mmol) of $AgSbF_6$ were added. After 1 h of reaction at RT, the solution was evaporated under reduced pressure to dryness. The addition of 5 mL of dichloromethane led to a yellow microcrystalline solid of **6** which was washed with Et_2O (1×5 mL) and vacuum-dried. Yield: 112.4 mg (0.092 mmol, 80%). Crystals suitable for X-ray analysis were obtained by slow evaporation of acetone solution at RT. Anal. calc. for $C_{62}H_{56}Ag_2Cl_4F_{24}N_6P_2Rh_2Sb_4$: C, 30.35; H, 2.30; N, 3.43. Found: C, 30.21; H, 2.17; N, 3.25. HRMS (μ-TOF): $C_{62}H_{56}Ag_2Cl_4F_{24}N_6P_2Rh_2Sb_4$, [1/2{M-2($SbF_6$)-Ag}]$^+$ calc. 646.0447, found 646.0444.

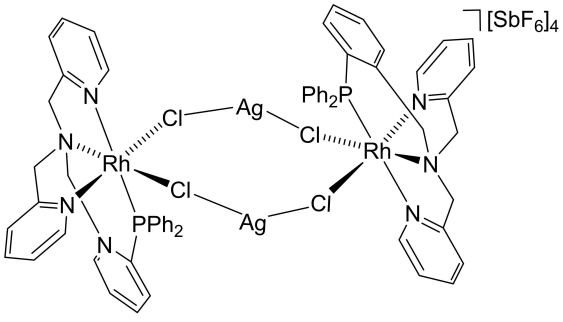

^{1}H NMR (400.16 MHz, acetone-d_6, RT, ppm): $\delta = 9.08$ (pseudo-triplet, $J = 4.6$ Hz, 1H, 6-CH(Py$_{transP}$)), 8.20 (d, $J = 5.9$ Hz, 1H, 6-CH(Py$_{cisP}$)), 8.17 (pseudo-td, $J = 7.7$, 1.3 Hz, 1H, 4-CH(Py$_{transP}$)), 8.02 (dd, $J = 11.6$, 8.1 Hz, 2H, 2×CH(Ar)), 7.97-7.89 (m, 3H, 2×CH(Ar), 3-CH(Py$_{transP}$)), 7.86 (pseudo-td, $J = 7.5$, 1.1 Hz, 1H, 4-CH(Py$_{cisP}$)), 7.72-7.45 (m, 7H, 6×CH-(Ar), 5-CH(Py$_{transP}$)), 7.32 (d, $J = 7.7$ Hz, 1H, 3-CH(Py$_{cisP}$)), 7.26 (m, 3H, 2×CH(Ar), 5-CH(Py$_{cisP}$)), 7.832 (pseudo-td, $J = 7.5$, 1.1 Hz, 1H, CH(Ar)), 7.15 (broad pseudo-triplet, $J = 79.9$ Hz, 2H, 2×CH(Ar)), 5.60 (d, $J =$ 16.0 Hz, 1H, CH_2(*pro-S*-Py$_{transP}$)), 5.49 (d, $J = 14.5$ Hz, 1H, CH_2(*pro-S*-P)), 5.41 (d, $J = 18.9$ Hz, 1H, CH_2(*pro-R*-Py$_{cisP}$)), 5.11 (d, $J = 15.8$ Hz, 1H, CH_2(*pro-R*-Py$_{transP}$)), 4.95 (d, $J = 18.9$ Hz, 1H, CH_2(*pro-S*-Py$_{cisP}$)), 4.82 (d, $J = 14.6$ Hz, 1H, CH_2(*pro-R*-P)). ^{13}C{^{1}H} NMR (100.62 MHz, acetone-d_6, RT, ppm): $\delta = 163.07$ (s, 2-C(Py$_{cisP}$)), 157.18 (d, $J = 2.4$ Hz, 1H 2-C(Py$_{transP}$)), 150.40 (s, 6-CH(Py$_{cisP}$)), 148.62 (s, 6-CH(Py$_{transP}$)), 141.89-121.95 (m, 24 C, C(Ar)), 75.43 (s, CH_2(Py$_{transP}$)), 67.97 (s, CH_2(Py$_{cisP}$)), 66.34 (d, $J = 4.9$ Hz, 2-CH_2(P)). ^{31}P{^{1}H} NMR (161.98 MHz, acetone-d_6, RT, ppm): $\delta = 28.73$ (d, $J = 103.9$ Hz). ^{31}P{^{1}H} NMR (161.98 MHz, solid, RT, ppm): $\delta = 28.83$ (brs).

[{Rh(κ^4-N$_2$N'P-L)}{Rh(COD)}(μ-Cl)$_2$][SbF$_6$]$_2$ (7)

To a solution of [$RhCl_2$(κ^4-*N$_2$N'P*-**L**)][SbF_6] (**1**) (100.0 mg, 0.113 mmol) in 40 mL of dry CH_2Cl_2, [Rh(COD)(NCMe)$_2$][SbF_6] (60.3 mg (0.114 mmol) was added. The resulting solution was stirred at RT for 40 min. After the partial evaporation of the solvent to 5 mL, the slow addition of Et_2O (10 mL) led to an orange microcrystalline solid. The crystals were separated by filtration, washed with Et_2O (1×5 mL), and vacuum dried. Yield: 95.7 mg (0.072 mmol, 64%). Crystals suitable for X-ray diffraction analysis were obtained by crystallisation from CH_2Cl_2/Et_2O solution at RT. Anal. calc. for $C_{39}H_{40}Cl_2F_{12}N_3PRh_2Sb_2$: C, 35.22; H, 3.03; N, 3.16. Found: C, 35.39; H, 3.14; N, 3.04. HRMS (μ-TOF) analysis was inconclusive because the bimetallic complex was cleaved, and the molecular peak corresponding to the fragment {$RhCl_2$(κ^4-*N$_2$N'P*-**L**)}. HRMS (μ-TOF): $C_{39}H_{40}Cl_2F_{12}N_3PRh_2Sb_2$, [M-2($SbF_6$)-Rh-COD]$^+$ calc. 646.0447, found 646.0445.

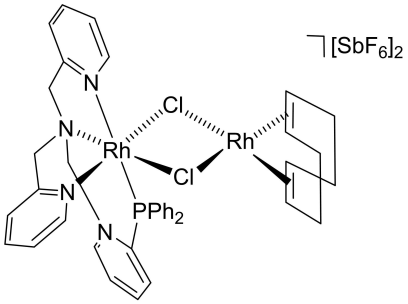

^{1}H NMR (400.16 MHz, CD_2Cl_2, RT, ppm): $\delta = 9.28$ (brs, 1H, 6-CH(Py$_{transP}$)), 7.51 (overlapped, 1H, 6-CH(Py$_{cisP}$)), 8.28-6.65 (m, 20H, CH(Ar)), 5.08 (brd, $J = 15.9$ Hz, 1H, CH_2(Pro-*S*-Py$_{transP}$)), 4.90 (brd, $J =$ 18.4 Hz, 1H, CH_2(Pro-*R*-Py$_{cisP}$)), 4.82 (d, $J = 16.3$ Hz, 1H, CH_2(Pro-*R*-Py$_{transP}$)), 4.76 (d, $J = 15.1$ Hz, 1H, CH_2(Pro-*S*-P)), 4.51 (d, $J = 18.9$ Hz, 1H, CH_2(Pro-*S*-Py$_{cisP}$)), 4.36 (d, $J = 18.8$ Hz, 1H, CH_2(Pro-*R*-P)), 4.28 (br, 2H, CH(COD)), 4.06 (br, 2H, CH(COD)), 2.31 (br, 4H, CH_2(COD)), 1.65 (br, 4H, CH_2(COD)). *^{13}C{^{1}H} NMR (100.62 MHz, CD_2Cl_2, RT, ppm):* $\delta =$ 160.72 (brs, 2-C(Py$_{cisP}$)), 155.00 (brs, 2-C(Py$_{transP}$)), 148.38 (brs, 6-CH(Py$_{cisP}$)), 148.03 (brs, 6-CH(Py$_{transP}$)), 142.07-122.17 (m, 24 C(Ar)), 81.36 (br, CH(COD)), 81.02 (br, CH(COD)), 74.56 (brs, CH_2(Py$_{transP}$)), 66.95 (brs, CH_2(Py$_{cisP}$)), 65.91 (brs, CH_2(P)), 30.44 (brs, CH_2(COD)), 30.33 (brs, CH_2(COD)). *^{31}P{^{1}H} NMR (161.98 MHz, CD_2Cl_2, RT, ppm):* $\delta =$ 27.28 (d, $J = 100.0$ Hz).

Supporting Information Summary

Crystal structure determinations are given in the Supporting Information. The authors have cited additional references within the Supporting Information.[25–31]

Note

This research was primarily conducted by undergraduate and master's students (I. B., I A., M. C., A. G. T., A. S.-J., C. B. and Z. A.).

Acknowledgements

We thank the Ministerio de Ciencia, Innovación y Universidades (MCIU) of Spain, Agencia Estatal de Investigación (AEI) of Spain, Fondo Europeo de Desarrollo Regional (FEDER) (CTQ2018-095561-BI00 and PID2021-122406NB–I00) and Gobierno de Aragón (Grupo de Referencia: Catálisis Homogénea Enantioselectiva E05_23R) for financial support. Some X-ray diffraction experiments were performed at XALOC beamline at ALBA Synchrotron with the collaboration of ALBA staff.

Conflict of Interests

The authors declare that they have no known competing financial interests or personal relationships that could have appeared to influence the work reported in this paper.

Data Availability Statement

The data that support the findings of this study are available in the supplementary material of this article.

Keywords: Rhodium · Ruthenium · Tetradentate ligand · Chiral-at-metal · Stereocontrol

[1] a) E. N. Jacobsen, A. Pfaltz, H. Yamamoto, Eds., *Comprehensive Asymmetric Catalysis*, Springer, Berlin, **1999**; b) I. Ojima, Ed., *Catalytic Asymmetric Synthesis*, Wiley, New York, NY Weinheim, **2000**; c) R. Noyori, *Asymmetric Catalysis in Organic Synthesis*, John Wiley and Sons, New York **1994**; d) P. J. Walsh, M. C. Kozlowski, *Fundamentals of Asymmetric Catalysis*, University Science Books, Sausalito **2009**.

[2] a) P. S. Steinlandt, L. Zhang, E. Meggers, *Chem. Rev.* **2023**, *123*, 4764–4794; b) R. Rodríguez, V. Passarelli, D. Carmona, in *Comprehensive Chirality*, Elsevier, **2024**, pp. 499–572; c) L. Zhang, E. Meggers, *Chem. Asian J.* **2017**, *12*, 2335–2342; d) L. Zhang, E. Meggers, *Acc. Chem. Res.* **2017**, *50*, 320–330; e) S. Akine, H. Miyake, *Coord. Chem. Rev.* **2022**, *468*, 214582; f) E. Meggers, *Chem. Eur. J.* **2010**, *16*, 752–758.

[3] a) M. Chavarot, S. Ménage, O. Hamelin, F. Charnay, J. Pécaut, M. Fontecave, *Inorg. Chem.* **2003**, *42*, 4810–4816; b) J. Hartung, R. H. Grubbs, *J. Am. Chem. Soc.* **2013**, *135*, 10183–10185; c) J. Hartung, P. K. Dornan, R. H. Grubbs, *J. Am. Chem. Soc.* **2014**, *136*, 13029–13037; d) K. Endo, Y. Liu, H. Ube, K. Nagata, M. Shionoya, *Nat. Commun.* **2020**, *11*, 6263; e) Y. Liu, H. Ube, K. Endo, M. Shionoya, *ACS Org. Inorg. Au* **2023**, *3*, 371–376; f) L. Hu, S. Lin, S. Li, Q. Kang, Y. Du, *ChemCatChem* **2020**, *12*, 118–121.

[4] A. Werner, *Chem. Ber.* **1911**, *44*, 1887–1898.

[5] a) C. Ganzmann, J. A. Gladysz, *Chem. Eur. J.* **2008**, *14*, 5397–5400; b) W. J. Maximuck, C. Ganzmann, S. Alvi, K. R. Hooda, J. A. Gladysz, *Dalton Trans.* **2020**, *49*, 3680–3691.

[6] a) H. Huo, C. Fu, K. Harms, E. Meggers, *J. Am. Chem. Soc.* **2014**, *136*, 2990–2993; b) C. Wang, L.-A. Chen, H. Huo, X. Shen, K. Harms, L. Gong, E. Meggers, *Chem. Sci.* **2015**, *6*, 1094–1100; c) C. Wang, L.-A. Chen, H. Huo, X. Shen, K. Harms, L. Gong, E. Meggers, *Chem. Sci.* **2015**, *6*, 1094–1100; d) L. Feng, X. Dai, E. Meggers, L. Gong, *Chem. Asian J.* **2017**, *12*, 963–967; e) C. Ye, S. Chen, F. Han, X. Xie, S. Ivlev, K. N. Houk, E. Meggers, *Angew. Chem. Int. Ed.* **2020**, *59*, 13552–13556; f) L. Hu, S. Lin, S. Li, Q. Kang, Y. Du, *ChemCatChem* **2020**, *12*, 118–121; g) H. Huo, X. Shen, C. Wang, L. Zhang, P. Röse, L.-A. Chen, K. Harms, M. Marsch, G. Hilt, E. Meggers, *Nature* **2014**, *515*, 100–103.h) H. Huo, K. Harms, E. Meggers, *J. Am. Chem. Soc.* **2016**, *138*, 6936–6939; i) J. Ma, X. Zhang, X. Huang, S. Luo, E. Meggers, *Nat. Protoc.* **2018**, *13*, 605–632; j) X. Huang, Q. Zhang, J. Lin, K. Harms, E. Meggers, *Nat. Catal.* **2018**, *2*, 34–40.

[7] Y. Zheng, Y. Tan, K. Harms, M. Marsch, R. Riedel, L. Zhang, E. Meggers, *J. Am. Chem. Soc.* **2017**, *139*, 4322–4325.

[8] Y. Hong, L. Jarrige, K. Harms, E. Meggers, *J. Am. Chem. Soc.* **2019**, *141*, 4569–4572.

[9] G. Wang, Z. Zhou, X. Shen, S. Ivlev, E. Meggers, *Chem. Commun.* **2020**, *56*, 7714–7717.

[10] a) M. Carmona, R. Rodríguez, V. Passarelli, F. J. Lahoz, P. García-Orduña, D. Carmona, *J. Am. Chem. Soc.* **2018**, *140*, 912–915; b) M. Carmona, R. Rodríguez, V. Passarelli, D. Carmona, *Organometallics* **2019**, *38*, 988–995; c) A. G. Tejero, M. Carmona, R. Rodríguez, F. Viguri, F. J. Lahoz, P. García-Orduña, D. Carmona, *RSC Adv.* **2022**, *12*, 34704–34714.

[11] M. Carmona, R. Rodríguez, I. Méndez, V. Passarelli, F. J. Lahoz, P. García-Orduña, D. Carmona, *Dalton Trans.* **2017**, *46*, 7332–7350.

[12] J. Téllez, I. Méndez, F. Viguri, R. Rodríguez, F. J. Lahoz, P. García-Orduña, D. Carmona, *Organometallics* **2018**, *37*, 3450–3464.

[13] A. G. Tejero, J. Castillo, F. Viguri, D. Carmona, V. Passarelli, F. J. Lahoz, P. García-Orduña, R. Rodríguez, *Chem. A Eur. J.* **2024**, *30*, e202303935.

[14] P. N. Liu, F. H. Su, T. B. Wen, H. H.-Y. Sung, I. D. Williams, G. Jia, *Chem. Eur. J.* **2010**, *16*, 7889–7897.

[15] a) R. S. Cahn, C. Ingold, V. Prelog, *Angew. Chem. Int. Ed. Engl.* **1966**, *5*, 385–415; b) V. Prelog, G. Helmchen, *Angew. Chem. Int. Ed. Engl.* **1982**, *21*, 567–583; c) C. Lecomte, Y. Dusausoy, J. Protas, J. Tirouflet, A. Dormond, *J. Organomet. Chem.* **1974**, *73*, 67–76. For the *CA* convention for octahedral centres see: d) N. G. Connelly, Royal Society of Chemistry (Great Britain), International Union of Pure and Applied Chemistry, Eds., *Nomenclature of Inorganic Chemistry. IUPAC Recommendations 2005*, Royal Society Of Chemistry Publishing/IUPAC, Cambridge, UK, **2005**.

[16] P. N. Liu, T. B. Wen, K. D. Ju, H. H.-Y. Sung, I. D. Williams, G. Jia, *Organometallics* **2011**, *30*, 2571–2580.

[17] Deposition numbers 2359688 (for **1**), 2359689 (for **2**), 2359690 (for **4**), 2359691 (for **5**), 2359692 (for **6**), and 2359693 (for **7**) contain the supplementary crystallographic data for this paper. These data are provided free of charge by the joint Cambridge Crystallographic Data Centre and Fachinformationszentrum Karlsruhe Access Structures service.

[18] B. J. Coe, S. J. Glenwright, *Coord. Chem. Rev.* **2000**, *203*, 5–80.

[19] G. Sipos, P. Gao, D. Foster, B. W. Skelton, A. N. Sobolev, R. Dorta, *Organometallics* **2017**, *36*, 801–817.

[20] M. Südfeld, W. S. Sheldrick, *Inorg. Chim. Acta* **2000**, *304*, 78–86.

[21] a) M. Carmona, L. Tejedor, R. Rodríguez, V. Passarelli, F. J. Lahoz, P. García-Orduña, D. Carmona, *Chem. A Eur. J.* **2017**, *23*, 14532–14546; b) M. Sudfeld, W. S. Sheldrick, *Z. Anorg. Allg. Chem.* **2002**, *628*, 1366–1372; c) X.-Y. Yi, T. C. H. Lam, Y.-K. Sau, Q.-F. Zhang, I. D. Williams, W.-H. Leung, *Inorg.Chem.* **2007**, *46*, 7193–7198.

[22] W. S. McNeil, D. D. DuMez, Y. Matano, S. Lovell, J. M. Mayer, *Organometallics* **1999**, *18*, 3715–3727.

[23] According to the Stokes–Einstein equation for spherical diffusing species [$D_X = (k_B T)/(6\pi h r_X)$, k_B is the Boltzmann constant, T is the temperature, h is the viscosity of the solvent and $_X$ is the name of the compound] the diffusion coefficient (D_X) is inversely proportional to the hydrodynamic radio(r_X). If two species ($_X$ = A and B) are considered, one (A) with a 2-fold hydrodynamic volume concerning the other (B), the ratio between the radii is $r_A/r_B = 2^{1/3} = 1.26$; therefore, $D_B/D_A = r_A/r_B = 1.26$.

[24] a) K. Polborn, K. Severin, *Eur. J. Inorg. Chem.* **1998**, *1998*, 1187–1192; b) G. Vlahopoulou, S. Moeller, J. Haak, P. Hasche, H. J. Drexler, D. Heller, T. Beweries, *Chem. Commun.* **2018**, *54*, 6292–6295; c) E. D. Amoateng, J. Zamora-Moreno, G. Kuchenbeiser, B. Donnadieu, F. Tham, V. Montiel-Palma, T. Keith Hollis, *J. Organomet. Chem.* **2022**, *997*, 122499; d) P.

Govender, S. Ngubane, B. Therrien, G. S. Smith, *J. Organomet. Chem.* **2017**, *848*, 281–287; e) S. Azpeitia, B. Fernández, M. A. Garralda, M. A. Huertos, *Eur. J. Inorg. Chem.* **2015**, *2015*, 5451–5456; f) J. Yao, W. T. Wong, G. Jia, *J. Organomet. Chem.* **2000**, *598*, 228–234.
[25] *SAINT+: Area-Detector Integration Software*, version 6.01; Bruker AXS: Madison, WI **2001**.
[26] a) G. M. Sheldrick, SADABS program; University of Göttingen: Göttingen, Germany, **1999**; b) L. Krause, R. Herbst-Irmer, G. M. Sheldrick, D. Stalke, *J. Appl. Cryst.* **2015**, *48*, 3–10.
[27] J. Juanhuix, F. Gil-Ortiz, G. Cuní, C. Colldelram, J. Nicolás, J. Lidón, E. Boter, C. Ruget, J. S. Ferrer Benach, *J. Synchrotron Radiat.* **2014**, *21*, 679–686.
[28] Agilent, CrysAlisPro v43. Agilent Technologies Ltd, Yarnton, Oxfordshire, England, **2014**.
[29] G. M. Sheldrick, *Acta Crystallogr.* **2008**, *A64*, 112–122.
[30] G. M. Sheldrick, *Acta Crystallogr.* **2015**, *C71*, 3–8.
[31] O. V. Dolomanov, L. J. Bourhis, R. J. Gildea, J. A. K. Howard, H. Puschmann, *J. Appl. Crystallogr.* **2009**, *42*, 339–341.

Manuscript received: June 11, 2024
Revised manuscript received: June 28, 2024
Accepted manuscript online: July 1, 2024
Version of record online: ■■, ■■

RESEARCH ARTICLE

Chiral-at-rhodium and ruthenium complexes have been synthesised with complete diastereoselectivity. This study explores the stereoselective chloride abstraction, highlighting the influence of metal centre charge and Lewis acidity. The ruthenium complex acts as a catalytic precursor by substituting both chloride ligands, while the rhodium complex operates as a ligand in Ag(I) and Rh(I) complexes *via* chlorine atoms.

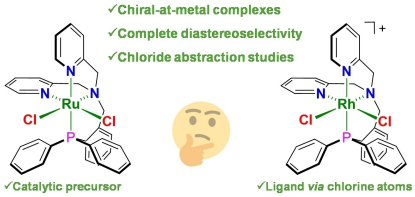

I. Barriendos, Í. Almárcegui, M. Carmona, A. G. Tejero, A. Soriano-Jarabo, C. Blas, Z. Aguado, D. Carmona, F. J. Lahoz, P. García-Orduña, F. Viguri, R. Rodríguez**

1 – 16

Stereocontrol of Metal-Centred Chirality in Rhodium(III) and Ruthenium(II) Complexes with $N_2N'P$ Ligand